## Title

Quantifying stimulus-response specificity to probe the functional state of macrophages



## Journal

Cell Systems, 14(3)

## ISSN

2405-4712

## Authors

Sheu, Katherine M
Guru, Aditya A
Hoffmann, Alexander

## Publication Date

2023-03-01

## DOI

10.1016/j.cels.2022.12.012

Peer reviewed

HHS Public Access

Author manuscript

*Cell Syst*. Author manuscript; available in PMC 2024 March 15.

Published in final edited form as:

*Cell Syst*. 2023 March 15; 14(3): 180–195.e5. doi:10.1016/j.cels.2022.12.012.

# Quantifying Stimulus-Response Specificity to probe the functional state of macrophages

**Katherine M. Sheu**[1], **Aditya A. Guru**[1], **Alexander Hoffmann**[1,2]

[1]Department of Microbiology, Immunology, and Molecular Genetics, and Institute for Quantitative and Computational Biosciences, University of California, Los Angeles, 611 Charles E. Young Dr S, Los Angeles, CA 90093.

[2]Lead Contact

## Abstract

Immune sentinel macrophages initiate responses to pathogens via hundreds of immune response genes. Each immune threat demands a tailored response, suggesting that the capacity for stimulus-specific gene expression is a key functional hallmark of healthy macrophages. To quantify this property, termed Response Specificity, we developed a single-cell experimental workflow and analytical approaches based on information theory and machine learning. We found that Response Specificity of macrophages is driven by combinations of specific immune genes that show low cell-to-cell heterogeneity and are targets of separate signaling pathways. The Response Specificity Profile, a systematic comparison of multiple stimulus response distributions, was distinctly altered by polarizing cytokines and enabled an assessment of the functional state of macrophages. Indeed, the Response Specificity Profile of peritoneal macrophages from old and obese mice showed characteristic differences, suggesting that Response Specificity may be a basis for measuring the functional state of innate immune cells.

## Graphical Abstract

Correspondence: ahoffmann@ucla.edu.

Author Contributions

KMS and AH designed the study. KMS performed the experiments and conducted the analyses. AG helped pilot the experimental approach and assisted with the machine learning analysis. KMS and AH wrote the paper. AH funded the work. All authors reviewed the manuscript.



Declaration of Interests

The authors are inventors on a provisional patent application related to this work, filed by UCLA.

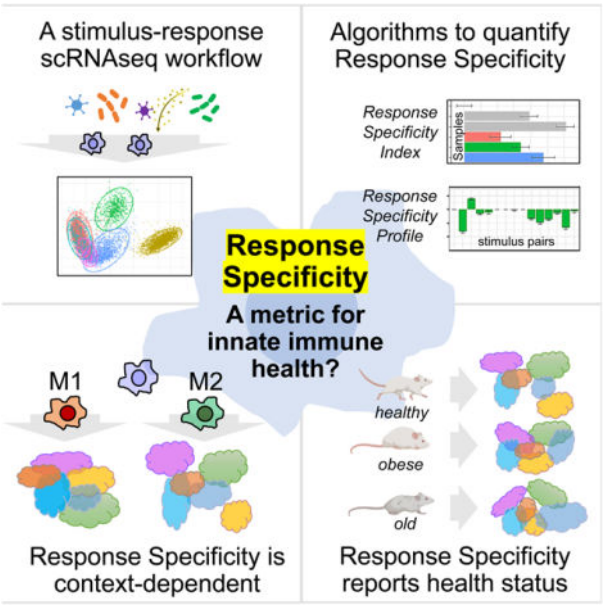


Emerging evidence suggest that macrophages are capable of immune threat-appropriate responses. To quantify Response Specificity, we introduce experimental and analytical workflows. Our studies reveal alterations by microenvironmental cytokines *in vitro* and within unhealthy mice, suggesting a means to assess the functional state of macrophages.

### Keywords

Response Specificity; macrophages; sentinel cells; information theory; machine learning; gene regulatory mechanisms; macrophage polarization; context dependence; innate immune function

## Introduction

Macrophages reside in almost all tissues of the body, where they are sensors for injury, infection, or disease[1]. The many functions they perform require them to respond appropriately to molecular patterns associated with pathogens (PAMPs), injury or danger (DAMPs), and to cytokines. Immune response genes code for potent bioactivities that are not constitutively expressed because they may be detrimental to the host. As such, immune response gene programs should only be deployed as needed and to the extent necessary. In fact, the precise deployment of immune response genes is critical for preventing abnormal immune sequelae. Both weak or overactive immune responses may arise from failure of immune sentinel cells to respond with appropriate specificity to immune threats, resulting in poor health outcomes[2–5].

Since immune sentinel cells function as individuals in initiating and coordinating immune responses, measuring their capacity to respond specifically to diverse pathogens requires consideration of their substantial cell-to-cell heterogeneity[6]. Prior population level macrophage transcriptome profiling studies identified a common immune response gene program[7], as well as gene programs that were in fact highly stimulus-specific[8–10]. A

plethora of population level studies have shown that specific responses arise from the signaling and epigenetic networks downstream of receptor-ligand interactions[11–13]. In addition, several studies measuring time-dependent stimulus responses using transcription factor knockouts have delineated the regulation of stimulus-dependent gene programs[8,13]. However, these studies did not quantify how specific macrophages responses actually are, as this requires single-cell measurements to determine the breadth and overlap of single-cell response distributions.

Macrophage heterogeneity itself has recently been studied *via* single-cell measurements in multiple contexts, such as during polarization or differentiation. For instance, the heterogeneity of macrophage populations after exposure to polarizing cytokines was shown to be greater if simultaneous conflicting cues were provided[14]. Single-cell heterogeneity has also been profiled during monocyte-to-macrophage differentiation in different tissues under different infection conditions, uncovering distinct activation paths *in vivo* that are altered by microenvironment and disease[15]. Importantly, macrophages must function as responders to immune threats, and thus recent studies have investigated the heterogeneity of single-cell macrophage or monocyte responses to single stimuli, after polarization[16] or after immune training[17]. However, these studies have not yet addressed how the heterogeneity of macrophage gene expression affects the specificity of responses to different to stimuli, and how the resulting stimulus-response specificity may be affected by different microenvironmental contexts.

The response of immune sentinels to stimuli is known to be a function of the microenvironmental context[18]. Polarizing cytokines enhance and diminish the activation of specific immune genes in an immune stimulus-specific manner by altering signaling networks and epigenetic landscapes[19–22]. Thus, aberrant cytokine contexts that are associated with inflammatory or immunological disease may affect the macrophage's capacity to mount stimulus-specific responses. Indeed, as macrophages circulate and patrol the body, profiling their capacities to mount stimulus-specific responses may report on the inflammatory state of their donor. However, in the absence of a workflow that measures response distributions and quantifies their overlap, the opportunity to leverage the macrophage's sensitivity to immune cytokines for reporting on the function of an individual's innate immune system has not been explored.

Here, we developed the necessary single-cell experimental and computational approaches to assess the functional states of macrophages, via quantification of the specificity of their responses to immune threats. Using information theoretic and machine learning approaches, we found that Response Specificity was driven by genes with narrow response distributions that in combination distinguished different ligands. Mechanistically, high Response Specificity was associated with stimulus-specific activation of IRF or MAPKp38 pathways, or differences in the dynamical profiles of NFκB signaling. We found that Response Specificity was affected by microenvironmental cytokines in a gene-specific manner. This realization prompted the development of the Response Specificity Profile, involving systematic pairwise comparisons, to reveal important functional distinctions in macrophages polarized *in vitro* or conditioned *in vivo* by inflammatory conditions of age or obesity.

## Results

### Despite single cell heterogeneity, macrophages produce highly specific gene expression responses to diverse immune stimuli

To quantify the degree of Response Specificity in macrophages, we developed an experimental workflow using a targeted mRNA sequencing approach[23] that was both cost-effective and reduced the technical noise of single-cell genome-wide RNA sequencing approaches (Fig. 1A). We selected a set of 500 macrophage genes via Principal Component Analysis on available macrophage response RNAseq data, which profiled macrophage responses across a time-series at 0, 1, 3, and 8hrs in response to 14 different viral and bacterial immune components or whole pathogens[8]. The gene loadings of the resulting PCA identified the most stimulus-specific genes in an unsupervised manner (Methods, Table S1, Fig. S1A). This bulk RNAseq dataset. The selected set of 500 genes showed greater enrichment of NFκB, IRF, and AP1 motifs than 1502 stimulus-induced genes, which suggested that these three signaling pathways are the primary drivers of Response Specificity (Fig. S1B).

To identify immune stimuli that would best represent Response Specificity, we further analyzed bulk RNAseq data from macrophages responding to 14 different pathogen or cytokine ligands to determine the ligands that induce diverse macrophage responses (Fig. S1A)[8]. Tensor components analysis[24] allowed an integrated decomposition of the data across all measured timepoints and stimuli, and showed that each ligand occupied a non-redundant location, indicating a distinct transcriptomic response at the population level. However, some ligands such as CpG and Pam3CSK sat closely adjacent in the tensor-decomposed space (Fig. S1C), indicating a greater similarity in their time-dependent expression profiles. From the 14 stimuli, we selected 6 with distinct tensor component weights that represented a spectrum of grampositive bacteria (Pam3CSK (P3C)), gram-negative bacteria (lipopolysaccharide (LPS)), bacterial DNA (CpG), viral nucleic acids (poly(I:C) (PIC)), and host cytokines activating either the interferon (IFNβ) or NFκB (TNF) signaling pathways.

Because gene programs are induced dynamically, the quantification of Response Specificity may depend on the time-point at which gene expression measurements are taken. To compare different timepoints of stimulation, we calculated pairwise stimuli distances at 1, 3, and 8hrs. Ligand-pair distances were most distinct at 3hrs (Fig. S1D), reflecting less impact from secondary signaling mechanisms than at the 8hr timepoint, and thus we chose the 3hr timepoint for our analysis of Response Specificity. A heatmap comparison of the newly generated single-cell data showed good concordance with the published bulk RNAseq data, while revealing substantial cell-to-cell heterogeneity in expression (Fig. 1B).

A comparison of the single-cell RNAseq data from our targeted approach (Rhapsody) to the genome-wide approach (10x Genomics) showed that both had similar concordance in their means to bulk data (Fig. S2A) and had comparable distributions to each other (Fig. S2B). Notably, the majority of genes captured only by the genome-wide approach were poorly expressed, further supporting utility of sequencing just the most informative genes through the targeted approach (Fig. S2C). For ~90% of the genes measured by both

approaches, the targeted approach also had a smaller percentage of cells with drop-out data (i.e. genes with zero reads), as each transcript could be sequenced more deeply (Fig. S2D). To avoid heterogeneity in macrophage populations due to different progenitors present in bone marrow, we used a clonal HoxB4-immortalized myeloid progenitor cell line that was differentiated into macrophages with macrophage-colony stimulating factor (M-CSF)-containing medium. The resulting cell populations showed similar bulk[25] and single-cell stimulus-response transcriptomic profiles as bone-marrow-derived macrophages (Fig. S3A–B). Taken together, these results suggested that the targeted sequencing approach provided a reproducible (Fig. S3C–D, Methods), cost-effective means for measuring heterogeneous single-cell macrophage gene expression in response to diverse immune ligands, making it suitable for quantifying Response Specificity.

To determine how much single-cell heterogeneity affected the stimulus-specificity of responses, we next sought to assess the overlap in gene expression response distributions. PCA revealed that IFNβ, LPS, and PIC response distributions were best distinguished, with minimal overlap of their 95% confidence regions on the first two components (44% variance explained), while TNF, CpG, and P3C appeared overlapping (Fig. 1C). UMAP on the top 20 components clarified that TNF could be separated from CpG and P3C on lower components (Fig. 1D), potentially because the latter activate stronger MAPK and non-oscillatory NFκB, while the MyD88mediated CpG and P3C response distributions remained largely indistinguishable (Fig. 1E). We trained a random forest classifier to determine how well the stimulus could be predicted given a single cell's response transcriptome (Fig. 1F, Fig. S4A–B). We found that IFNβ could be perfectly predicted (F1 score = 100%), while the bacterial ligands CpG and P3C were confused with each other and were thus more poorly classified (F1 = 85% and 74%, respectively). The overall prediction accuracy of 88% across all stimuli indicated a high degree of stimulus-specificity despite cell-to-cell heterogeneity in macrophage responses to ligands (Fig. 1F).

## High stimulus-specificity is determined by combinations of individual genes that alone can distinguish only subsets of stimulus pairs

To identify genes that may be driving the observed stimulus-specificity, we next employed an information theoretic approach[26,27]. We considered ligand information as transmitted through a channel comprised of cell signaling and gene regulatory networks, both affected by pre-existing biological heterogeneity and the stochasticity of biochemical reactions, to produce heterogeneous gene expression responses (Fig. 2A)[28,29]. Under this framework, the maximum mutual information (max MI) describes the certainty about the ligand input given the transcriptome output. One bit equates perfect distinguishability of two ligand response distributions ($2^{\mathbf{1}} = 2$), 2 bits for 4 ligands ($2^{\mathbf{2}} = 4$), and 2.58 bits for 6 ligands ($2^{\mathbf{2.58}} = 6$). Because mutual information is maximized over all possible input distributions (max MI), this metric provides a comparable absolute quantity for the biological characteristic of Response Specificity that is independent of the underlying type of data distribution or the mechanisms by which the information is encoded.

We found that 95% of the measured genes on their own conveyed no more than 1 bit of information (Fig. 2B, Table S2), or ability to distinguish two conditions. A heatmap of the

top-ranking individual genes indicated that rather than each gene having several levels of expression that would separate ligands, most genes displayed an on-or-off expression pattern across single cells, which thus distinguishes only two groups of ligands (Fig. 2C). The single gene most informative for distinguishing stimuli was *Cmpk2*, a mitochondria-associated gene with reported antiviral and homeostatic functions[30,31], which allowed for a maximum mutual information of 1.5 bits (Fig. 2C, Table S2), corresponding to expression distributions sufficiently narrow to define approximately 3 kinds of stimulus-specific responses.

How then can macrophages achieve high Response Specificity? One possibility is that a combination of genes that show low cell-to-cell heterogeneity may specify stimulus-specific responses to multiple stimuli. To assess this possibility, we employed the same information theoretic framework to calculate the maximum mutual information provided by the best-performing combinations of genes. Indeed, the best combination of two genes (*Cmpk2* and *Nfkbiz*) already allowed for a maximum MI of almost 2 bits, with the gain in max MI plateauing to ~2.25 bits as larger combinations were tested (Fig. 2D). Interestingly, the majority of genes within the top gene combinations were intracellular proteins controlling nucleotide metabolism (*Cmpk2*)[32], anti-viral activity and cell death (*Ifit3*, *Ifit1*, *Mx2*)[33–35], ubiquitination (*Peli1*)[36], mRNA half-life of inflammatory genes (*Zc3h12a*)[37], or phagocytosis (*Swap70*)[38] (Figure 2E). Cytokine genes commonly measured by antibody-based assays (*Tnf*, *Cxcl10*, *Ccl5*, *Ccl2*) had secondary roles (Table S3). Machine learning classification using different gene combination sizes confirmed these conclusions. Even just the top two genes performed reasonably well at 70% accuracy, the top 5 genes further improved classification accuracy to 78%, and the top 15 genes performed almost as well as all genes at 85% accuracy (vs. 88% for all) (Fig. 2F, cf. Fig. 1F). Gene combinations that worked well together did so by distinguishing complementary ligand pairs (Fig. 2G). For example, *Nfkbiz* alone contributed 0.75 bits to distinguishing CpG and PIC, complementing the inability of *Cmpk2* expression to distinguish these ligands (0 bits).

## The Response Specificity of cytokine genes is limited by high cell-to-cell heterogeneity, despite having distinct expression means

High Response Specificity requires not only that mean population gene expression is distinct, but also that the cell-to-cell heterogeneity is low such that distributions of single cell responses have limited overlap. Hence, we investigated whether Response Specificity was limited by small differences in means or wide distributions. We found that mean squared deviation (MSD), which summarizes differences in means across ligands, correlated more strongly to Response Specificity ($r = 0.8$) than average Fano factor, which summarizes average gene heterogeneity ($r = -0.5$) (Fig. 3A). However, a few outliers were evident: some genes with high mean difference (e.g. *Ccl5* or *Cxcl10*) showed unimpressive Response Specificity, with similar max MI to genes with low mean difference (e.g. *Ifi205*) (Fig. 3A). Plotting the average Fano Factor revealed that these outliers differed in their dispersion: *Cxcl10* and *Ccl5* displayed much higher heterogeneity (i.e. high avg. Fano factors) (Fig. 3B). In contrast, metabolic and non-secreted genes such as *Cmpk2*, *Ifi205*, and *Ifit3* had tight distributions (i.e. unusually low avg. Fano factors), and thus high Response Specificity.

Interestingly, a pattern emerged where the Fano Factors of cytokine/chemokine genes were higher than expected, diminishing their Response Specificity despite distinct mean expression levels (Fig. 3C). For example, directly plotting the response distributions of cytokines *Ccl5*, *Tnf*, *Cxcl10* (Fig. 3D), as well as the non-cytokine gene *Cmpk2*, showed that *Ccl5* was induced with high variance expression distributions in response to PIC, P3CSK, and CpG, while *Cxcl10* and *Tnf* distributions also had Fano Factors (variance/mean ratio) close to or above one for multiple stimuli, which meant that their distributions were broad in relation to mean expression. In contrast, the Fano Factors across stimuli for the non-cytokine gene *Cmpk2* were well below one for all stimuli (Fig. 3E). These results suggested that single cell cytokine/chemokine expression may have limited predictive value in specifying distinct ligand-responses due to single cell heterogeneity.

## The stimulus specificities of immune response genes are due to selective deployment of IRF and p38 pathways, and NFκB dynamical features

In macrophage responses, four signaling pathways and their downstream gene regulatory factors are combinatorially activated and are responsible for transmitting information about extracellular ligands to the nucleus (Fig. 4A). Their target genes have been categorized into five gene regulatory strategies, namely AP1, NFκB, IRF, NFκB|p38, and NFκB|IRF[8]. We asked which gene regulatory strategies may mediate the high Response Specificity of particular genes, as measured by max MI. We assigned each gene to a regulatory logic through matching mathematical model simulations of possible regulatory logics to available stimulus-response datasets, followed by a curation of prior literature (Table S4, Fig. S5A, Methods). The appropriate motifs were enriched for genes assigned to each of the clusters (Fig. S5B). We then calculated the max MI of every gene for ligand pairs (Fig. 4B–D,). For example, contrasting TNF vs. IFNβ, genes within every regulatory logic group showed high specificity (Fig. 4B), a reflection of the fact that each group is activated by only one of the ligands: AP1 and NFκB and NFkB|p38 are activated by TNF but not IFNβ, while IRF genes are activated by IFNβ but not TNF.

In contrast, for the P3CSK vs. TNF stimulus pair, only NFκB|p38 target genes showed specificity because both stimuli activate AP1 and NFκB, fail to activate IRF, and differ in the extent of p38 activation (Fig. 4C). Similarly, for P3CSK vs. PIC, NFκB|p38 targets showed specificity because PIC does not activate p38[8]. However, for P3CSK vs. PIC unlike P3CSK vs. TNF, IRF target genes also contributed to the Response Specificity since PIC activates IRF but P3CSK does not (Fig. 4D). Of note, the max MI of IRF target genes was on average lower for P3CSK vs. PIC than for TNF vs IFNβ, potentially due to highly heterogeneous activation of IRF by the TRIF signaling pathway[39].

In addition to combinatorial pathway control, the dynamics of NFκB activation also specify gene expression[40]. Stimulus-specific NFκB temporal dynamics involve six NFκB signaling codons that convey information about the stimulus to target genes: “Speed”, “Peak Amplitude”, “Oscillations”, “Duration”, “Total Activity”, and “Early vs. Late” activity (Fig. 4e)[41]. To determine which signaling codons may be associated with the stimulus-specificity of NFκB target genes, we correlated pairwise specificities of NFκB signaling codons with the pairwise specificities of NFκB target genes (Fig. S5C). We found that NFκB target genes

differed in which signaling codons they were associated with (Fig. 4F, Fig. S5D). These distinctions may be reflective of genes employing distinct gene regulatory mechanisms such as an incoherent feedforward loop that decodes "Peak Amplitude"[42], long mRNA half-life or slow chromatin opening steps that decode "Duration"[43], or the requirement for *de novo* enhancers that distinguishes "Oscillations"[44].

## Cytokine polarization modulates the Response Specificity of specific genes to specific stimuli

Macrophages show remarkable functional pleiotropy that is dependent on microenvironmental context[45]. Thus, polarization by prior cytokine exposure may alter their capacity for stimulus-specific responses. To test this hypothesis, we polarized macrophages into M1(IFNγ) and M2(IL4) states that represent opposing ends of the macrophage polarization spectrum (Fig. S6A)[46], and generated single-cell stimulus response data for the six ligands (Fig. 5A). Polarized M1(IFNγ) and M2(IL4) macrophages expressed macrophage marker *Adgre1* (Fig. S6B) and the appropriate polarization markers (Fig. S6C–D). PCA and UMAP projections of response distributions revealed that stimulus responses for polarized macrophages were distinct (Fig. 5B, Fig. S6E), but M1(IFNγ) response distributions were more overlapping than those for M0 naïve macrophages.

We found that Response Specificity was reduced in both polarization states for every set of the best gene combinations, as calculated by max MI, indicating that polarized macrophages may function more as specialized effectors and less as sentinels that serve a primary role of distinguishing immune threats (Fig. 5C, Table S3). Interestingly, we further observed that the genes within each of the best gene sets were different for each polarization state (Fig. 5D). This was corroborated by examining one gene, *Cxcl10*, which was included in the best gene combinations in M0 and M2(IL4) conditions but not in M1(IFNγ). Indeed, in M1(IFNγ) macrophages, *Cxcl10* was promiscuously rather than stimulus-specifically activated, and no longer carried stimulus-specific information about any pairs of stimuli (Fig. 5E). This change in Response Specificity could be ascribed to the IRF pathway. Several NFκB|IRF target genes (*Cxcl10*, *Cmpk2*, *Ifit3*, and *Trim21*) lost specificity in M1(IFNγ) macrophages (Fig. 5F, Fig. S6F), reflecting the fact that in the presence of IFNγ conditioning such genes only require activation of NFκB to be induced. In fact, using the random forest machine learning model trained on M0 naïve macrophages to predict the stimuli seen by M1 or M2 cells, we found that M1 responses were all more likely to be predicted as LPS or PIC, which are IRF-activating stimuli (Fig. 5G). Gene ontology attributed this loss of Response Specificity to the biological pathways "response to virus", "response to LPS", and "response to IFNβ" (Fig. S6G, Table S5). Motif enrichment analysis also identified IRF target genes as responsible (Fig. 5H).

While a global analysis indicated that polarization diminished macrophage Response Specificity, the genes most affected differed for each macrophage state. In addition, a smaller set of largely NFκB response genes also showed increased rather than diminished Response Specificities under each polarization condition (Fig. 5F). Such nuanced findings preclude the use of a single gene or even a single set of genes to quantify Response Specificity over multiple macrophage states. The Response Specificity of macrophages thus

may not be appropriately characterized by a single number, but rather a higher dimensional profile.

## The Response Specificity Profile of stimulus pairs assesses the functional state of macrophages, and readily distinguishes M0 vs. M1 vs. M2 macrophages

We noted that while different macrophage states could be identified by profiling their steady state transcriptomes (Fig. S6A), their responses to stimuli were even more distinguishable (Fig. 6A). Quantifying the distance between both the stimulated and unstimulated distributions, we found that in all comparisons, specific stimuli revealed differences that were not as evident from steady state measurements. This was especially evident for M0 vs. M2 macrophages, whose response distributions to Pam3CSK and CpG were particularly more distinct than could be ascertained from steady-state distributions (Fig. 6B). This illustrates that for assessing the functional state of macrophages, measurements of multiple stimulus responses provide non-redundant information.

To quantitatively assess the Response Specificity provided by all 6 stimuli, we developed an approach to profile the max MI of all 15 stimulus pairs within the macrophage response landscape characterized by a PCA projection of all single-cell stimulus-response transcriptomes (Fig. 6C, Table S6, Methods). The resulting Response Specificity Profile of M0, M1(IFNγ), and M2(IL4) macrophages showed specific differences for some of the stimulus pairs tested (Fig. 6C). Particularly, M1(IFNγ) macrophages were impaired in distinguishing bacterial stimuli (LPS-CpG; LPS-P3C), while M2(IL4) macrophages were not. Meanwhile, M2(IL4) macrophages were more impaired in distinguishing host-cytokine vs. bacteria (TNF-CpG, TNF-P3C). In both polarization states, CpG-P3CSK specificity, which had been the least distinguishable stimulus pair for M0 macrophages, was enhanced.

Calculating the difference in max MI from the M0 state, and thereby the Delta Response Specificity Profile, provided a characteristic signature of the functional state of the macrophage (Fig. 6D). This profile could also be summarized succinctly in a single number, the delta Response Specificity Index (ΔRSI), which provided a clearer indication of differences among polarization states than the mutual information calculated on all stimuli together (Fig. 6E). We found that the overall ΔRSI of M2(IL4) macrophages was greater than that of M1(IFNγ) macrophages, as a result of M2(IL4) macrophages showing a greater loss of specificity in distinguishing host vs. bacterial ligands. Thus, the Response Specificity Profile and ΔRSI revealed a signature of pairwise response specificity scores associated with the function of each macrophage type, whether naïve, M1(IFNγ) or M2(IL4).

## Peritoneal macrophages from old and obese mice show distinctive alterations in their Response Specificity Profiles

Next, we tested whether the Response Specificity Profile might reveal aberrations in macrophages derived from mice with conditions associated with inflammatory disease. We took peritoneal macrophages (PMs) from healthy mice (17 weeks old), old mice (90 weeks old), and high-fat-diet obese mice (17 weeks old) and performed the Response Specificity workflow using five ligands: LPS, TNF, PIC, P3C, and IFNβ (Fig. 7A). Visualization of the resulting single-cell data suggested that old mice had aberrant IFNβ-response distributions,

while obese mice had aberrant PIC-response distributions (Fig. 7B). We calculated the Response Specificities for the data (Fig. 7C) and noted that the PMs from young, healthy mice had an overall ΔRSI most similar to naïve M0 macrophages (Fig. 7D). A closer inspection of the Response Specificity Profile showed that PMs from old mice showed the most diminished specificity for IFN-activating stimulus pairs (e.g. LPS-PIC), akin to what we observed with M1(IFNγ) macrophages. PMs from high-fat diet obese mice had decreased specificity across all stimulus pairs, but particularly in distinguishing cytokine vs. viral (TNF-PIC) responses. The differences observed through calculation of the Response Specificity Profile on stimulus subsets suggests an importance to comparing multiple subsets of stimuli in evaluating innate immune function.

To identify individual genes that showed particularly high losses of Response Specificity in these *in-vivo*-conditioned macrophages, we compared max MI values for each gene (Fig. 7E). We found that macrophages from both old and obese mice lost specificity in the cytokine *Tnf*, but also in metabolic gene *Acod1*[47,48], and upstream TLR signaling network proteins such as *Peli1*[36], *Nfkbiz*[49,50], and *Phlda1*[51]. Normal function of these genes has been implicated in resistance to septic shock, macrophage response to atherosclerosis, and protection from autoimmune disease. Interestingly, a couple of genes showed higher stimulus-specificity in these dysregulated microenvironments. In old mice, genes with the highest gains in specificity were the cytokine *Cxcl10* and cytokine regulator *Aw112010*, which is required for mucosal immunity[52]; and in obese mice, *Cav1* and *Slamf8*, which play roles in macrophage differentiation and migration[53,54]. This suggested that macrophage responses in unhealthy mice deviated from healthy through both losses and gains of stimulus-specificity in individual genes: Losses indicating responses that are too promiscuous potentially causing conditions for autoimmunity to arise, and gains indicating responses that are too restricted to a particular stimulus, potentially diminishing core functions of macrophages in innate defenses or resolution of tissue inflammation and damage.

As peritoneal macrophages of mice of different ages may be composed of different subpopulations, we next evaluated to what extent the changes in Response Specificity may be due to subpopulations of macrophages differentially present in diseased vs. healthy mice. Based on scRNAseq of steady-state populations[55], we found that all subclusters of macrophages were found in both young and old mice (Fig. S7A–E), though in slightly different proportions (Fig. S7F). Using marker genes to match these clusters to the stimulus-response data, we likewise found these subgroups represented across healthy, aged, and obese mice, though again in different proportions (Fig. S7G).

Taken together, quantifying the Response Specificity of macrophages revealed that this functional hallmark of immune sentinel cells is affected not only by polarizing cytokines used in pre-conditioning regimes *in vitro*, but also by the microenvironments *in vivo* that are evidently distinct in obese and old mice. It is possible that Response Specificity profiles of peritoneal macrophages captures altered responses of both distinct subpopulations of macrophages that are differentially represented in inflammatory conditions and distinct functional states of the same subpopulation. Regardless, the observed differences

in Response Specificity suggest that quantifying post-stimulation single-cell response distributions could be valuable for assessing innate immune function.

## Discussion

Mounting stimulus-appropriate immune responses is a key property of healthy macrophage function[7,8,56–58]. Macrophage Response Specificity is a function of the stimulus-specific engagement of signaling pathways and may be diminished by molecular network noise that results in cell-to-cell heterogeneity. While Response Specificity of the macrophage NFκB signaling pathway has been characterized[41,59], the Response Specificity of immune gene expression responses arising from all macrophage signaling pathways has not yet been quantified. By developing the experimental and computational tools to do so, we found that the high gene expression specificity observed was generated by sufficiently narrow response distributions in combinations of genes that respond with distinct patterns across stimuli, but that the contribution of often-measured cytokine genes was limited by high cell-to-cell heterogeneity of expression. Mechanistically, we found that Response Specificity is generated by stimulus-specific activation of interferon or MAPKp38 signaling, or by differences in NFκB dynamics. Loss of IRF gene specificity by microenvironmental polarization was the key driver in altering Response Specificity Profiles. Given that Response Specificity is context-dependent, we profiled peritoneal macrophages from old and obese mice, revealing highly specific changes in the Response Specificity Profile that correlated with a different health status. These findings may prompt further studies to investigate whether macrophage Response Specificity could be a means to characterize the innate immune health of human donors.

Our ability to measure and subsequently quantify Response Specificity was enabled by a quantitative assay for cost-effective, reliable scRNAseq[23,60]. The targeted sequencing approach we pursued here resulted in less technical noise than genome-wide approaches, due to improved reverse transcriptase efficiency and increased sequencing depth per gene[23,61]. However, even with technical improvements, the remaining measurement noise[62] still may result in underestimates of the true Response Specificity. Future efforts on smaller gene lists may allow the use of even less noisy measurement approaches like single molecule fluorescence *in situ* hybridization (smFISH)[63,64], that capitalize on the smaller sets of informative genes identified in this study.

Measuring the responses from macrophages rather than their steady-state transcriptomes provided additional levels of information. First, we found that stimulus-response transcriptomes may reveal differences in macrophage populations that are not apparent in the steady state. This may be because exposure histories and cytokine contexts change signaling pathways and chromatin states that are not reflected in steady-state mRNA abundances. Measuring stimulus responses also allowed us to evaluate multiple distributions for each macrophage type, rather than the single distribution provided by profiling the steady state. Emergent from these multiple distributions is Response Specificity, which evaluates the relative extent of distribution overlap and reports on the ability of each macrophage type to distinguish among immune threats. Not only is Response Specificity an important biological hallmark property of macrophages[58], but also from the workflow perspective, it

being based on multiple measurements that may be compared with each other makes this analysis metric more resistant to technical noise or batch effect, potentially enabling better comparisons across studies.

The information theoretic approach we used here to quantify Response Specificity, previously employed to quantify the information transmission capacity of signaling pathways[28,41,59,65–70]. In fact, we found that Response Specificity of individual genes can be traced either to a single pathway or by multiple pathways[8], for example the NFκB target gene *Tnf* whose mRNA half-life is regulated by stimulus-induced MAPKp38[71]. This combinatorial control explains why in principle some single genes like *Tnf* can hold more information than available from a single signaling pathway. But even single pathway genes may show Response Specificity owing to their ability to distinguish different dynamical characteristics, such as NFκB signaling codons. Interestingly, we observed that such genes correlated strongly to identifiable signaling codons, indicating that their gene regulatory strategies are able to decode the information present in the stimulus-specific deployment of the signaling codon.

Theoretically, information loss from signaling to gene expression is minimal without noise[72,73], while with noise, maintaining minimal information loss is only possible under select optimal promoter or chromatin conditions[74–76]. Specifically, to achieve high gene expression Response Specificity, signaling information must be interpreted by gene regulatory strategies[77,78] without amplifying the cell-to-cell heterogeneity in signaling activity[79], and also without introducing further heterogeneity through pre-existing chromatin heterogeneity[80,81] or molecular noise[82–85]. In this context, it is not surprising that the Response Specificity of most individual genes was low. However, as macrophages do not rely on only a single gene to mount a biological response to a specific immune threat, even with information loss at each particular promoter, the overall Response Specificity observed through combinations of a few genes from complementary pathways was still high.

Within the body, macrophages are exposed to polarizing microenvironments in physiological scenarios[86], as well as in pathological inflammatory contexts such as aging or obesity[87–89]. As circulating cells they are potentially reporters of even localized infections[90]. Indeed, profiling the transcriptome or epigenome of circulating cells or macrophages has revealed molecular markers or signatures that are prognostic for therapeutic efficacy[91,92] or alternative disease courses, such as in persistent infectious or inflammatory disease[15,93], cardiovascular and autoimmune diseases[94–98]. However, as seen in human COVID-19 studies, it can be unclear which individuals have poor or vigorous immune health until they are challenged by infection[99–103]. Here, we considered that macrophage functions are deployed in response to immune threats and that stimulus responses are a function not only of the steady-state transcriptome or epigenome but also the dynamics of signaling complexes, membranes, and transport rates. We reasoned that macrophage responses to different stimuli reveal a functional pleiotropy not evident at steady state, and that the stimulus-specific deployment of functions is key to healthy immunity. Indeed, we found that macrophages conditioned *in vitro* by defined polarizing cytokines, as well as macrophages isolated from obese or old mice, showed distinctly altered Response Specificity profiles due to both cytokine genes and regulators within macrophage metabolic and signaling pathways.

In developing the Response Specificity Profile, we found that analyzing single genes and pairs of stimuli provided more insight than aggregating the data together. For example, Response Specificity for each pair of stimuli differed for each polarization condition, but this information is lost when calculating mutual information for all stimuli at once. Instead, an aggregate score of alterations in the Response Specificity Profile (delta RSI) provide a first indication of differences, and the full Response Specificity Profile pinpointed aberrancies in select stimulus pairs that may be a diagnostic for a specific condition, such as macrophages from obese mice confusing TNF and PIC responses. For initial surveys of Response Specificity Profiles, measuring the expression of a large number of genes in response to multiple stimuli is important, as the most informative genes and stimulus comparisons are different across various macrophage states[104]. We employed a PCA approach to characterize the response landscape and identify genes important across conditions, using the gene weights in principal components. Indeed, the Response Specificity of individual genes differed greatly between the two disease models tested here, emphasizing the importance of gene-by-gene analysis in characterizing the Response Specificity Profile to make biologically meaningful predictions.

Characterizing the macrophage Response Specificity Profile may prove useful in clinical scenarios. Many steady-state metrics of immune health exist, such as the complete blood count that is a mainstay of clinical lab tests. However, tests for functional immune responses, already used in select clinical scenarios such as tuberculosis testing or allergy testing, are also rapidly emerging[105]. Multiple such assays rely on *ex vivo* stimulation of extracted clinical samples to diagnose immunosuppression[106] or phagocytic ability[107], and have included transcriptomic profiling studies of stimulus-responses on peripheral blood that identified inter-individual variation among healthy donors and the genes driving those differences[108]. As seen with existing assays, to what extent stimulus-response measurements provide more reliably prognostic information than steady-state molecular profiling may depend on the health condition being studied.

Our assay of single cell macrophage responses may identify outlier response cells within each donor sample through the Response Specificity Profile, that may be associated with risk for aberrant inflammatory responses or diminished innate immune defenses, or that may be reflective of an ongoing inflammatory or infectious condition that is not otherwise presented. The Response Specificity Profile allows new samples to be compared readily to a healthy range, a property which could be the basis for a clinically deployable measure of innate immune health. The stimulus-response data may also identify specific genes with aberrant response distributions in patient cohorts or in individual donors. Identifying such genes may provide cost-effective prognostic markers for specific cohorts or point to the underlying etiology of poor immune function. To realize this promise, large-scale clinical studies will be required to establish connections between Response Specificity Profiles and risk for disease. However, as a quantifiable property of macrophage function that changes with conditioning cytokines or states of health and disease, macrophage Response Specificity Profile may be a viable approach for measuring the health of innate immune function in the clinic.

# STAR METHODS

## RESOURCE AVAILABILITY

**Lead Contact:** Further information and requests for resources and reagents should be directed to and will be fulfilled by the Lead Contact, Alexander Hoffmann (ahoffmann@ucla.edu).

**Materials Availability:** This study did not generate new materials.

**Data and Code Availability:**

- Data have been deposited at Zenodo and GEO and are publicly available as of the date of publication. DOIs are listed in the key resources table.
- All original code has been deposited on the Github repository https://github.com/signalingsystemslab/ResponseSpecificity and is publicly available as of the date of publication. The DOI of an archived version is listed in the key resources table. This includes code for data processing and analysis, and processed single cell data, including raw and normalized counts.
- Any additional information required to reanalyze the data reported in this paper is available from the lead contact upon request.

## EXPERIMENTAL MODEL AND SUBJECT DETAILS

**Macrophage Cell Culture—**Macrophages were obtained by differentiating immortalized myeloid progenitors (HoxB4 iMPs)[25]. The choice of using HoxB4 immortalized progenitors was multifold: First, Singh et al., 2022 showed that HoxB4-iMPDMs (immortalized myeloid progenitor-derived macrophages) had gene expression responses more similar to BMDMs than RAW cells to BMDMs, thus making the HoxB4-iMPDMs a better choice to model primary macrophages than the current most popularly used murine macrophage line, RAW 264.7. Second, using iMPDMs removed the need for using large numbers of mice, making it more economical and animal-friendly. Third, while introduction of HoxB4 may be a concern in terms of the function of the macrophage, the near-clonal nature of the precursor cells rather than the mixture of various precursors in bone marrow may in fact be an advantage. HoxB4-iMPs were differentiated in DMEM/10% FBS + 30% L929 supernatant for a total of 10 days: iMPs were initially thawed into 10cm non-adherent petri dishes for 3 days. On day 0 of differentiation, cells were then washed once and transferred into differentiation media (DMEM/10% FBS, 30% L929 supernatant, 1% PS, 1% L-Glut, b-Me (1:1000)). Cells were replated into 6cm plates with new media on day 7, at a density of ~20k cells/$cm^2$. On day 10, the iMP-derived macrophages (iMPDMs) were stimulated with 100ng/mL lipopolysaccharide (LPS, Sigma Aldrich), 10ng/mL murine TNF, and 50μg/mL low molecular weight polyinosine-polycytidylic acid (Poly(I:C)), 100nM synthetic CpG ODN 1668 (CpG), 500U/ml IFNβ, or media only Untreated control. For polarized macrophages, cells were incubated in 50ng/ml IFNγ or 50ng/ml IL4 for 24 hours prior to stimulation on day 10.

**Peritoneal Macrophage Experiments—**All mouse work was done following institutional approval under UCLA's accreditation by Association for Assessment and Accreditation of Laboratory Animal Care International (AAALAC). C57Bl/6 mice were obtained from Jackson labs. Two male mice were combined for each condition in order to obtain sufficient numbers of cells for the assay: 90wks old (000664 C57BL/6J), 17wks old (380050 C57BL/6J/DIO high fat diet (60% fat diet)), 17wks old (380056 C57BL/6J/DIO controls (10% fat diet)). Peritoneal macrophages were extracted by injecting 10mL PBS +1% FBS into the peritoneal space, shaking gently, and then pulling out as much fluid as possible, typically ~8ml. Macrophages were plated in DMEM +10%FBS and allowed to rest 24hrs. Floating cells after that time were washed away, and remaining adherent macrophages were stimulated with the same ligand concentrations as for iMPDMs: 100ng/mL lipopolysaccharide (LPS, Sigma Aldrich), 10ng/mL murine TNF (R&D), 50μg/mL low molecular weight polyinosine-polycytidylic acid (Poly(I:C)), 500U/ml IFNβ, or media only Untreated control. Cells were washed once with cold PBS after 3hrs of stimulation and lifted into suspension for the Rhapsody scRNAseq assay. The investigators were not blinded the identity of the animal models during the experiments or outcome assessment.

## METHOD DETAILS

**Gene Panel Selection Algorithm—**To select genes for single-cell targeted gene profiling, we analyzed existing bulk transcriptomic profiling of macrophage responses. Bulk RNAseq data from Cheng et al, 2017 was obtained from GEO GSE68318. Counts were converted to counts per million (cpm) using the package *edgeR*[111], and genes with cpm>4 in at least three samples were retained. Induced genes were gathered by calculating fold changes at each of the 14 stimulus conditions available in the dataset, at each timepoint, against the unstimulated controls. Genes were retained as induced genes if they met the threshold of log2(fold change)>2 and p-value < $10^{-5}$, which resulted in 1502 genes.

Because PCA identifies a new basis that maximizes variance within the rotated data, it was ideal for identifying genes that varied in expression level across different stimuli. PCA was performed centered and unscaled on the induced genes across all time points for the 14 stimuli in the dataset. The loadings matrix obtained from the PCA was used to calculate a rank score for each gene. The rank was computed as the radial distance of each gene $j$ from the origin, over the top 20 PCs: $\text{score}_j = \sum_{x=1}^{20} (PCx_j)^2$, where $PCx_j$ is the component $x$ loadings value for gene $j$. The top 480 ranked genes were included in the panel, and the remaining 20 genes were manually selected to add genes such as cell type markers, macrophage polarization markers, and transcription factors (Table S1). As a visual confirmation of the approach, k-means clustering was performed on all induced genes and loadings were colored by cluster. As expected, genes with the highest absolute loadings values in each principal component tended to be spread across different clusters, and the top genes in each principal component exhibited distinct patterns across stimuli.

**Selection of Stimuli for Response Specificity Assay—**To identify an optimal set of the most distinct stimuli from the set of 14 used in the bulk transcriptomic data, tensor components analysis (TCA) was performed. TCA is a higher dimensional parallel of PCA –

whereas PCA is performed on a *genes* × *sample* matrix, TCA is performed on a higher-order tensor by folding the gene expression matrix into a *genes* × *stimuli* × *timepoint* tensor. The bulk RNAseq data consisted of $N$ genes over $S$ stimuli with $T$ timepoints per stimulus, which formed a third-order tensor $\boldsymbol{X}$ of dimensions $N \times S \times T$ (a three-dimensional array). Tucker decomposition[116] was performed using the package *rTensor*. This decomposes the tensor into a core tensor $G$ of dimensions $R_1 \times R_2 \times R_3$, multiplied by a matrix $U^{(i)}$ along each mode,

$$\boldsymbol{X} = G \times_1 \mathrm{U}^{(1)} \times_2 U^{(2)} \times_3 U^{(3)}$$

The first five components, which explained 92% of the variance in the data, were retained. The stimulus loadings matrix $U^{(2)}$ of dimensions $S \times R_2$ was hierarchically clustered on the first five components, and stimuli that each occupied separate branches of the hierarchical tree were selected. Stimuli that represented whole bacterial organisms or viruses were not selected, in favor of isolated bacterial or viral components.

**Rhapsody scRNAseq—**To collect the adherent macrophages for scRNAseq using the Rhapsody platform, macrophage cells were washed 1x with cold PBS, then lifted into suspension by incubating at 37C for 5 minutes with Accutase, which resulted in cell viability typically >85%. Cells were centrifuged at 4C, 400g for 5 minutes, and resuspended in PBS + 2% FBS. Cells were hash-tagged with antiCD45-hashtags (BD Rhapsody # 633793) and loaded onto the cartridge following manufacturer's instructions (BD Rhapsody # 633771), with the following modifications, which helped ensure sufficient cell viability for the subsequent steps: Incubation with hashtags was performed for 30mins on ice, instead of 20mins at room temperature; only two washes were performed after hashtag incubation to minimize cell loss. Each cartridge was then loaded with a total of ~36k cells across 12 hash-tagged samples (~3k cells/sample). Libraries were prepared according to manufacturer's instructions (BD Rhapsody # 633771) and sequenced 2×100 on Novaseq 6000.

## QUANTIFICATION AND STATISTICAL ANALYSIS

**Motif Enrichment—**Motif enrichment of induced genes and selected genes was performed using HOMER[112], with a motif search range of −1000 to +100 of the TSS of each gene. Individual motif hits were placed into five categories: bZIP (AP1 family TF motifs), IRF (IRF and ISRE motifs), RHD (Rel Homology Domain NFκB family motifs), ETS (Erythroblast Transformation Specific family TF motifs), and Zf (Zinc finger motifs). To summarize the overall enrichment of particular transcription factor families within the gene sets, the average −ln(p value) of motifs in each category was calculated, and a second log transform was taken for plot visualization.

**Gene Ontology—**Gene ontology on selected genes versus unselected genes was performed using *clusterProfiler*[114] against a background of all genes. Cutoff values of p-value < 0.01, Benjamini-Hochberg q-value <0.05, and minimum gene set size >5 were used. Ontologies were grouped if they had a similarity proportion greater than 0.7. The top three Biological Processes ontology terms for each group were plotted.

**scRNAseq Data Processing—**Raw fastq files were processed using the BD Rhapsody™ Targeted Analysis Pipeline (version v1.0)[23] hosted on Seven Bridges Genomics. Distribution-Based Error Correction (DBEC)-adjusted UMI counts (molecules per cell) were used in the downstream analysis. Multiplets, cells with undetermined barcodes, and cells with less than 80 features were removed from the analysis. Due to the selected 500 gene panel comprised of largely inducible genes, the assumption that the total number of RNAs per cell is constant does not hold. Counts were therefore normalized using the package *ISnorm*[115], rather than the more standard approach of dividing by total counts per cell. PCA was performed centered and unscaled using the R function *prcomp*, and UMAP and tSNE were performed on the top 20 PCs.

**Assignment of Genes to Regulatory Mechanisms—**We first pursued a data-driven approach for the assignment, by examining time-series cell population average data from macrophages stimulated with the six stimuli. We then simulated the 7 gene regulatory logics identified by (Cheng et al, 2017), collapsing short and long mRNA half-life clusters. Each of the ordinary differential equations used for the 7 regulatory logics followed the same general form:

$$\frac{dmRNA}{\{dt\}} = k_{syn} f(t) - k_{deg} * mRNA,$$

where for single transcription factor logic gates[8],

$$f(t) = (1 - k_0) * \frac{(K_D * [TF(t)])^n}{1 + (K_D * [TF(t)])^n} + k_0$$

and for two transcription factor OR logic gates[8],

$$f(t) = (1 - k_0) * \frac{(K_{D_1} * TF1(t))^n + (K_{D_2} * TF2(t))^n + (K_{D_1} * K_{D_2} * TF1(t) * TF2(t))^n}{1 + (K_{D_1} * TF1(t))^n + (K_{D_2} * TF2(t))^n + (K_{D_1} * K_{D_2} * TF1(t) * TF2(t))^n)} + k_0$$

We matched regulatory logics to each gene by assigning the GRS with the lowest RMSD between model and experimental data (see https://github.com/signalingsystemslab/ResponseSpecificity;[8,117]). We then manually curated the model assignments based on evidence provided by the literature, resulting in assignments given in Table S4.

**Machine Learning Models and Feature Importance—**Machine learning classification models were trained using scRNAseq data from naïve macrophages. The data was split 70%/30% into a training group and a testing group. Using only the training data, a random forest model was trained using repeated 10-fold cross validation, with 3 repeats. The parameter *mtry*, which is the number of variables randomly selected as candidate features for each decision tree split, was set to √(total number of features). As alternative models, weighted k-nearest neighbors and neural network model were also trained on the same dataset. Random forest, weighted kNN, and neural network models were implemented using the R package *caret (classification and regression training)*[109]. After the model was trained,

the remaining held-out data was tested, with each cell assigned a soft probability prediction for each ligand. The highest probability ligand was the final prediction. Ensemble modeling was performed by majority voting, taking the predicted stimuli from each of the individual models and choosing the most common stimulus predicted for each cell among the different machine learning models. Macrophages of other polarization conditions, M1(IFNγ) and M2(IL4), were tested using the model trained on M0 naïve macrophages.

Feature importance was extracted from the trained random forest model, which is calculated by how much information is lost at each node/split of the decision trees. We calculated this value based on Gini impurity: $\sum_{i=1}^{C}(freq_i \times (1 - freq_i))$, across all unique category labels $C$. The feature importance is then the product (decrease in node impurity) * (probability of reaching that node), scaled so the top feature has a value of 100.

**Mutual Information Analyses—**An information theoretic approach was used to identify either individual genes or combinations of genes providing the highest maximum mutual information between ligand identity and gene expression. Error bars on mutual information calculations were done using 10 bootstraps on 50% of the data. Estimation of maximum mutual information was implemented using the R package *SLEMI*[67], which uses a statistical learning-based approach to more accurately and more efficiently calculate maximum mutual information for data types with higher dimensional outputs. The max MI was first calculated for each gene individually, using all stimuli (highest theoretical max MI = 2.58bits), as well as for all pairs of stimuli (highest theoretical max MI = 1.0bits). To relate the max MI to the either the mean and variance of each gene, max MI was plotted against either the average Fano factor $\left(avg \cdot FF = \left(\sum_{i=1}^{S}\left(\frac{\sigma_i}{\mu_i}\right)\right)/S\right)$ across all stimuli S for each gene, or the mean squared deviation $\left(\text{MSD} = \frac{\sum_{i=1}^{S}(x_i - \bar{x})^2}{S}\right)$.

To estimate the maximum mutual information of the best combination of 1, 2, 3, …, $N$ genes, we first started from a list of the top 20 genes that individually had the best max MI value. For each of these single dimension channels, we scanned every combination of two genes, and again ranked the best combination of two genes and retained the top 20. This process was repeated for each additional gene until the gain in max MI for each additional gene leveled off. Retaining only the top 20 sets at each dimension made the calculation more computationally feasible, while still allowing the possibility for gene combinations that are not simply additive of the previous dimension's highest max MI combination.

For gene-specific pairwise calculation of MI, max MI between pairs of stimuli was calculated for each gene at 3hrs using the single-cell RNAseq data. Max MI was plotted against gene regulatory groups between the two stimuli. Correlation coefficients were calculated using the max MI values for signaling pairs for every NFκB signaling codon, and the max MI values for the corresponding gene expression pairs for every NFκB target gene. Genes without any correlation p-value < 0.25 across the six codons were removed from the display. The Pearson's coefficient was plotted on the heatmap, and genes were hierarchically clustered using complete linkage.

**Response Specificity Profile—**The Response Specificity Profile is a collection of values that collectively summarize the distinguishability of macrophage responses to different stimuli. The response landscape on which the Response Specificity Profile is calculated was obtained first by principal component analysis performed centered and unscaled on all stimuli across M0, M1(IFNγ), and M2(IL4) cells. This initial matrix can be written as $\boldsymbol{M} = N \times P$, where N is the total number of measured genes and P is the stimulated single cells of different macrophage subtypes. This matrix rotation of $\boldsymbol{M}$ by PCA represents the landscape of physiological macrophage responses. Calculation of maximum mutual information using the PC scores was then performed for all possible pairs of stimuli. The advantage of using PC scores to perform mutual information analyses lies in the reduction of noise that would otherwise result in overfitting. Overfitting due to the large number of features was observed to result in saturation of the maximum mutual information values to the theoretical maximum for all pairs. Max MI was therefore calculated on the top three PCs (capturing 42% of the variance in the data), using a truncation based on the PCA scree plot, as each subsequent component after Component 5 added only ~1% more to the variance explained. All error bars were generated by 50 iterations of 50% bootstrap resampling of the complete single cell dataset.

The Response Specificity Profile of new samples were evaluated by projection of the new gene expression data onto the dimensionality-reduced space. Letting the initial PCA be defined as $\boldsymbol{S} = \boldsymbol{W}^{\boldsymbol{T}} \times \boldsymbol{M}$, where $\boldsymbol{S}$ is the $r \times P$ scores matrix, and $\boldsymbol{W}$ is the $N \times r$ loadings matrix, the scores of the new projected data is then given by

$$S_{new} = W^T \times M_{new}.$$

Since cells from disease models are projected into the same basis, scores from any new projected data now sit in the same lower-dimensional space and can be compared to the Response Specificity of samples within initially defined response landscape. For new samples, the maximum mutual information between ligand and transcriptomic output was again calculated for all available pairs of ligands using the PC scores. The summary score delta Response Specificity Index (ΔRSI) was generated by the following: $\Delta\text{RSI} = \sqrt{\Sigma}\left(RSI_p - RSI_p^{M0}\right)^2$ across all pairs of stimuli $p$.

## Supplementary Material

Refer to Web version on PubMed Central for supplementary material.

## Acknowledgements

We thank lab members Ying Tang and Diane Lefaudeux for helpful comments, and Supriya Sen and Carolina Chavez for reagents and experimental and analysis assistance. We thank Jessica Li (UCLA) for support and advice. KMS was supported by the UCLA Medical Scientist Training Program (T32-GM008042) and Systems and Integrative Biology Training Grant (T32-GM008185). The work was funded by R01AI127864 and R01GM12507 to AH. Cartoon mouse icons were created with BioRender. Sequencing data from this paper was performed with the services of the UCLA Technology Center for Genomics and Bioinformatics Sequencing Core.

## Inclusion and Diversity

While citing references scientifically relevant for this work, we also actively worked to promote gender balance in our reference list.

## References:


1. Murray PJ, and Wynn TA (2011). Protective and pathogenic functions of macrophage subsets. Nature Reviews Immunology 11, 723–737. 10.1038/nri3073.
2. Alleva DG, Pavlovich RP, Grant C, Kaser SB, and Beller DI (2000). Aberrant macrophage cytokine production is a conserved feature among autoimmune-prone mouse strains: elevated interleukin (IL)-12 and an imbalance in tumor necrosis factor-alpha and IL-10 define a unique cytokine profile in macrophages from young nonobese diabetic mice. Diabetes 49, 1106–1115. 10.2337/diabetes.49.7.1106. [PubMed: 10909966]
3. Galani I-E, Rovina N, Lampropoulou V, Triantafyllia V, Manioudaki M, Pavlos E, Koukaki E, Fragkou PC, Panou V, Rapti V, et al. (2021). Untuned antiviral immunity in COVID-19 revealed by temporal type I/III interferon patterns and flu comparison. Nature Immunology 22, 32–40. 10.1038/s41590-020-00840-x. [PubMed: 33277638]
4. McKechnie JL, and Blish CA (2020). The Innate Immune System: Fighting on the Front Lines or Fanning the Flames of COVID-19? Cell Host & Microbe 27, 863–869. 10.1016/j.chom.2020.05.009. [PubMed: 32464098]
5. Moore JB, and June CH (2020). Cytokine release syndrome in severe COVID-19. Science 368, 473–474. 10.1126/science.abb8925. [PubMed: 32303591]
6. Muldoon JJ, Chuang Y, Bagheri N, and Leonard JN (2020). Macrophages employ quorum licensing to regulate collective activation. Nat Commun 11, 1–14. 10.1038/s41467-020-14547-y. [PubMed: 31911652]
7. Nau GJ, Richmond JFL, Schlesinger A, Jennings EG, Lander ES, and Young RA (2002). Human macrophage activation programs induced by bacterial pathogens. Proceedings of the National Academy of Sciences 99, 1503–1508. 10.1073/pnas.022649799.
8. Cheng CS, Behar MS, Suryawanshi GW, Feldman KE, Spreafico R, and Hoffmann A (2017). Iterative Modeling Reveals Evidence of Sequential Transcriptional Control Mechanisms. Cell Systems 4, 330–343.e5. 10.1016/j.cels.2017.01.012. [PubMed: 28237795]
9. Sheu KM, Luecke S, and Hoffmann A (2019). Stimulus-specificity in the responses of immune sentinel cells. Current Opinion in Systems Biology 18, 53–61. 10.1016/j.coisb.2019.10.011. [PubMed: 32864512]
10. Xue J, Schmidt SV, Sander J, Draffehn A, Krebs W, Quester I, De Nardo D, Gohel TD, Emde M, Schmidleithner L, et al. (2014). Transcriptome-Based Network Analysis Reveals a Spectrum Model of Human Macrophage Activation. Immunity 40, 274–288. 10.1016/j.immuni.2014.01.006. [PubMed: 24530056]
11. Gottschalk RA, Martins AJ, Angermann BR, Dutta B, Ng CE, Uderhardt S, Tsang JS, Fraser IDC, Meier-Schellersheim M, and Germain RN (2016). Distinct NF-κB and MAPK Activation Thresholds Uncouple Steady-State Microbe Sensing from Anti-pathogen Inflammatory Responses. Cell Systems 2, 378–390. 10.1016/j.cels.2016.04.016. [PubMed: 27237739]
12. Luecke S, Sheu KM, and Hoffmann A (2021). Stimulus-specific responses in innate immunity: Multilayered regulatory circuits. Immunity 54, 1915–1932. 10.1016/j.immuni.2021.08.018. [PubMed: 34525335]
13. Tong AJ, Liu X, Thomas BJ, Lissner MM, Baker MR, Senagolage MD, Allred AL, Barish GD, and Smale ST (2016). A Stringent Systems Approach Uncovers Gene-Specific Mechanisms Regulating Inflammation. Cell 165, 165–179. 10.1016/j.cell.2016.01.020. [PubMed: 26924576]
14. Muñoz-Rojas AR, Kelsey I, Pappalardo JL, Chen M, and Miller-Jensen K (2021). Co-stimulation with opposing macrophage polarization cues leads to orthogonal secretion programs in individual cells. Nature Communications 12, 301. 10.1038/s41467-020-20540-2.
15. Sanin DE, Ge Y, Marinkovic E, Kabat AM, Castoldi A, Caputa G, Grzes KM, Curtis JD, Thompson EA, Willenborg S, et al. (2022). A common framework of monocyte-

derived macrophage activation. Science Immunology 7, eabl7482. 10.1126/sciimmunol.abl7482. [PubMed: 35427180]

16. Dichtl S, Sanin DE, Koss CK, Willenborg S, Petzold A, Tanzer MC, Dahl A, Kabat AM, Lindenthal L, Zeitler L, et al. (2022). Gene-selective transcription promotes the inhibition of tissue reparative macrophages by TNF. Life Sci Alliance 5, e202101315. 10.26508/lsa.202101315. [PubMed: 35027468]
17. Zhang B, Moorlag SJCFM, Dominguez-Andres J, Bulut Ö, Kilic G, Liu Z, Crevel R. van, Xu C-J, Joosten LAB, Netea MG, et al. (2022). Single-cell RNA sequencing reveals induction of distinct trained-immunity programs in human monocytes. J Clin Invest 132. 10.1172/JCI147719.
18. Ginhoux F, Schultze JL, Murray PJ, Ochando J, and Biswas SK (2016). New insights into the multidimensional concept of macrophage ontogeny, activation and function. Nat Immunol 17, 34–40. 10.1038/ni.3324. [PubMed: 26681460]
19. Cheng Q, Behzadi F, Sen S, Ohta S, Spreafico R, Teles R, Modlin RL, and Hoffmann A (2019). Sequential conditioning-stimulation reveals distinct gene- and stimulus-specific effects of Type I and II IFN on human macrophage functions. Scientific Reports 9, 5288. 10.1038/s41598-019-40503-y. [PubMed: 30918279]
20. Kang K, Bachu M, Park SH, Kang K, Bae S, Park-Min K-H, and Ivashkiv LB (2019). IFN-γ selectively suppresses a subset of TLR4-activated genes and enhancers to potentiate macrophage activation. Nature Communications 10, 3320. 10.1038/s41467-019-11147-3.
21. Lawrence T, and Natoli G (2011). Transcriptional regulation of macrophage polarization: enabling diversity with identity. Nature Reviews Immunology 11, 750–761. 10.1038/nri3088.
22. Mitchell S, Mercado EL, Adelaja A, Ho JQ, Cheng QJ, Ghosh G, and Hoffmann A (2019). An NFκB Activity Calculator to Delineate Signaling Crosstalk: Type I and II Interferons Enhance NFκB via Distinct Mechanisms. Front Immunol 10, 1425. 10.3389/fimmu.2019.01425. [PubMed: 31293585]
23. Shum EY, Walczak EM, Chang C, and Christina Fan H (2019). Quantitation of mRNA Transcripts and Proteins Using the BD Rhapsody™ Single-Cell Analysis System. Adv. Exp. Med. Biol 1129, 63–79. 10.1007/978-981-13-6037-4_5. [PubMed: 30968361]
24. Kolda TG, and Bader BW (2009). Tensor Decompositions and Applications. SIAM Rev. 51, 455–500. 10.1137/07070111X.
25. Singh A, Sen S, Adelaja A, and Hoffmann A (2022). Stimulus-Response signaling dynamics characterize macrophage polarization states. 2022.03.27.485991. 10.1101/2022.03.27.485991.
26. Cover TM, and Thomas JA (2012). Elements of Information Theory (John Wiley & Sons).
27. Shannon CE (1948). A mathematical theory of communication. The Bell System Technical Journal 27, 379–423. 10.1002/j.1538-7305.1948.tb01338.x.
28. Suderman R, Bachman JA, Smith A, Sorger PK, and Deeds EJ (2017). Fundamental trade-offs between information flow in single cells and cellular populations. PNAS 114, 5755–5760. 10.1073/pnas.1615660114. [PubMed: 28500273]
29. Tkačik G, Callan CG, and Bialek W (2008). Information flow and optimization in transcriptional regulation. PNAS 105, 12265–12270. 10.1073/pnas.0806077105. [PubMed: 18719112]
30. Lai J-H, Wu D-W, Wu C-H, Hung L-F, Huang C-Y, Ka S-M, Chen A, Chang Z-F, and Ho L-J (2021). Mitochondrial CMPK2 mediates immunomodulatory and antiviral activities through IFN-dependent and IFN-independent pathways. iScience 24, 102498. 10.1016/j.isci.2021.102498. [PubMed: 34142025]
31. Arumugam P, Chauhan M, Rajeev T, Chakraborty R, Shankaran D, Ramalingam S, Gandotra S, and Rao V (2021). The mitochondrial gene CMPK2 functions as a rheostat for macrophage homeostasis in inflammation. 2021.11.01.466732. 10.1101/2021.11.01.466732.
32. Xu Y, Johansson M, and Karlsson A (2008). Human UMP-CMP kinase 2, a novel nucleoside monophosphate kinase localized in mitochondria. J Biol Chem 283, 1563–1571. 10.1074/jbc.M707997200. [PubMed: 17999954]
33. Hsu Y-L, Shi S-F, Wu W-L, Ho L-J, and Lai J-H (2013). Protective roles of interferon-induced protein with tetratricopeptide repeats 3 (IFIT3) in dengue virus infection of human lung epithelial cells. PLoS One 8, e79518. 10.1371/journal.pone.0079518. [PubMed: 24223959]

34. Pidugu VK, Pidugu HB, Wu M-M, Liu C-J, and Lee T-C (2019). Emerging Functions of Human IFIT Proteins in Cancer. Front Mol Biosci 6, 148. 10.3389/fmolb.2019.00148. [PubMed: 31921891]
35. Betancor G, Jimenez-Guardeño JM, Lynham S, Antrobus R, Khan H, Sobala A, Dicks MDJ, and Malim MH (2021). MX2-mediated innate immunity against HIV-1 is regulated by serine phosphorylation. Nat Microbiol 6, 1031–1042. 10.1038/s41564-021-00937-5. [PubMed: 34282309]
36. Chang M, Jin W, and Sun S-C (2009). Peli1 facilitates TRIF-dependent Toll-like receptor signaling and proinflammatory cytokine production. Nat Immunol 10, 1089–1095. 10.1038/ni.1777. [PubMed: 19734906]
37. Matsushita K, Takeuchi O, Standley DM, Kumagai Y, Kawagoe T, Miyake T, Satoh T, Kato H, Tsujimura T, Nakamura H, et al. (2009). Zc3h12a is an RNase essential for controlling immune responses by regulating mRNA decay. Nature 458, 1185–1190. 10.1038/nature07924. [PubMed: 19322177]
38. Baranov MV, Revelo NH, Dingjan I, Maraspini R, Ter Beest M, Honigmann A, and van den Bogaart G (2016). SWAP70 Organizes the Actin Cytoskeleton and Is Essential for Phagocytosis. Cell Rep 17, 1518–1531. 10.1016/j.celrep.2016.10.021. [PubMed: 27806292]
39. Cheng Z, Taylor B, Ourthiague DR, and Hoffmann A (2015). Distinct single-cell signaling characteristics are conferred by the MyD88 and TRIF pathways during TLR4 activation. Sci. Signal 8, ra69–ra69. 10.1126/scisignal.aaa5208. [PubMed: 26175492]
40. Behar M, and Hoffmann A (2010). Understanding the temporal codes of intra-cellular signals. Current Opinion in Genetics & Development 20, 684–693. 10.1016/j.gde.2010.09.007. [PubMed: 20956081]
41. Adelaja A, Taylor B, Sheu KM, Liu Y, Luecke S, and Hoffmann A (2021). Six distinct NFκB signaling codons convey discrete information to distinguish stimuli and enable appropriate macrophage responses. Immunity 54, 916–930.e7. 10.1016/j.immuni.2021.04.011. [PubMed: 33979588]
42. Lee RE, Walker SR, Savery K, Frank DA, and Gaudet S (2014). Fold change of nuclear NF-kappaB determines TNF-induced transcription in single cells. Mol Cell 53, 867–879. 10.1016/j.molcel.2014.01.026. [PubMed: 24530305]
43. Sen S, Cheng Z, Sheu KM, Chen YH, and Hoffmann A (2020). Gene Regulatory Strategies that Decode the Duration of NFκB Dynamics Contribute to LPS- versus TNF-Specific Gene Expression. Cell Syst 10, 169–182.e5. 10.1016/j.cels.2019.12.004. [PubMed: 31972132]
44. Cheng QJ, Ohta S, Sheu KM, Spreafico R, Adelaja A, Taylor B, and Hoffmann A (2021). NF-κB dynamics determine the stimulus specificity of epigenomic reprogramming in macrophages. Science 372, 1349–1353. 10.1126/science.abc0269. [PubMed: 34140389]
45. Murray PJ (2017). Macrophage Polarization. Annual Review of Physiology 79, 541–566. 10.1146/annurev-physiol-022516-034339.
46. Murray PJ, Allen JE, Biswas SK, Fisher EA, Gilroy DW, Goerdt S, Gordon S, Hamilton JA, Ivashkiv LB, Lawrence T, et al. (2014). Macrophage Activation and Polarization: Nomenclature and Experimental Guidelines. Immunity 41, 14–20. 10.1016/j.immuni.2014.06.008. [PubMed: 25035950]
47. Li Y, Zhang P, Wang C, Han C, Meng J, Liu X, Xu S, Li N, Wang Q, Shi X, et al. (2013). Immune Responsive Gene 1 (IRG1) Promotes Endotoxin Tolerance by Increasing A20 Expression in Macrophages through Reactive Oxygen Species. J Biol Chem 288, 16225–16234. 10.1074/jbc.M113.454538. [PubMed: 23609450]
48. Sun KA, Li Y, Meliton AY, Woods PS, Kimmig LM, Cetin-Atalay R, Hamanaka RB, and Mutlu GM Endogenous itaconate is not required for particulate matter-induced NRF2 expression or inflammatory response. eLife 9, e54877. 10.7554/eLife.54877. [PubMed: 32255424]
49. Kakiuchi N, Yoshida K, Uchino M, Kihara T, Akaki K, Inoue Y, Kawada K, Nagayama S, Yokoyama A, Yamamoto S, et al. (2019). Frequent mutations that converge on the NFKBIZ pathway in ulcerative colitis. Nature, 1–6. 10.1038/s41586-019-1856-1.
50. Okuma A, Hoshino K, Ohba T, Fukushi S, Aiba S, Akira S, Ono M, Kaisho T, and Muta T (2013). Enhanced Apoptosis by Disruption of the STAT3-IκB-ζ Signaling Pathway in Epithelial

Cells Induces Sjögren's Syndrome-like Autoimmune Disease. Immunity 38, 450–460. 10.1016/j.immuni.2012.11.016. [PubMed: 23453632]

51. Lyu JH, Huang B, Park D-W, and Baek S-H (2016). Regulation of PHLDA1 Expression by JAK2-ERK1/2-STAT3 Signaling Pathway. J Cell Biochem 117, 483–490. 10.1002/jcb.25296. [PubMed: 26239656]
52. Jackson R, Kroehling L, Khitun A, Bailis W, Jarret A, York AG, Khan OM, Brewer JR, Skadow MH, Duizer C, et al. (2018). The translation of non-canonical open reading frames controls mucosal immunity. Nature 564, 434–438. 10.1038/s41586-018-0794-7. [PubMed: 30542152]
53. Fu Y, Moore X-L, Lee MKS, Fernández-Rojo MA, Parat M-O, Parton RG, Meikle PJ, Sviridov D, and Chin-Dusting JPF (2012). Caveolin-1 plays a critical role in the differentiation of monocytes into macrophages. Arterioscler Thromb Vasc Biol 32, e117–125. 10.1161/ATVBAHA.112.254151. [PubMed: 22772753]
54. Wang G, Driel B.J. van, Liao G, O'Keeffe MS, Halibozek PJ, Flipse J, Yigit B, Azcutia V, Luscinskas FW, Wang N, et al. (2015). Migration of Myeloid Cells during Inflammation Is Differentially Regulated by the Cell Surface Receptors Slamf1 and Slamf8. PLOS ONE 10, e0121968. 10.1371/journal.pone.0121968. [PubMed: 25799045]
55. Mogilenko DA, Shpynov O, Andhey PS, Arthur L, Swain A, Esaulova E, Brioschi S, Shchukina I, Kerndl M, Bambouskova M, et al. (2021). Comprehensive Profiling of an Aging Immune System Reveals Clonal GZMK+ CD8+ T Cells as Conserved Hallmark of Inflammaging. Immunity 54, 99–115.e12. 10.1016/j.immuni.2020.11.005. [PubMed: 33271118]
56. Hajishengallis G, and Lambris JD (2011). Microbial manipulation of receptor crosstalk in innate immunity. Nat Rev Immunol 11, 187–200. 10.1038/nri2918. [PubMed: 21350579]
57. Rivera A, Siracusa MC, Yap GS, and Gause WC (2016). Innate cell communication kick-starts pathogen-specific immunity. Nat Immunol 17, 356–363. 10.1038/ni.3375. [PubMed: 27002843]
58. Sheu KM, and Hoffmann A (2022). Functional Hallmarks of Healthy Macrophage Responses: Their Regulatory Basis and Disease Relevance. Annu Rev Immunol 40, 295–321. 10.1146/annurev-immunol-101320-031555. [PubMed: 35471841]
59. Selimkhanov J, Taylor B, Yao J, Pilko A, Albeck J, Hoffmann A, Tsimring L, and Wollman R (2014). Accurate information transmission through dynamic biochemical signaling networks. Science 346, 1370–1373. 10.1126/science.1254933. [PubMed: 25504722]
60. Mair F, Erickson JR, Voillet V, Simoni Y, Bi T, Tyznik AJ, Martin J, Gottardo R, Newell EW, and Prlic M (2020). A Targeted Multi-omic Analysis Approach Measures Protein Expression and Low-Abundance Transcripts on the Single-Cell Level. Cell Reports 31, 107499. 10.1016/j.celrep.2020.03.063. [PubMed: 32268080]
61. Ey S, Em W, C C, and H CF (2019). Quantitation of mRNA Transcripts and Proteins Using the BD Rhapsody™ Single-Cell Analysis System. Adv Exp Med Biol 1129, 63–79. 10.1007/978-981-13-6037-4_5. [PubMed: 30968361]
62. Jiang R, Sun T, Song D, and Li JJ (2022). Statistics or biology: the zero-inflation controversy about scRNA-seq data. Genome Biology 23, 31. 10.1186/s13059-022-02601-5. [PubMed: 35063006]
63. Foreman R, and Wollman R (2020). Mammalian gene expression variability is explained by underlying cell state. Molecular Systems Biology 16. 10.15252/msb.20199146.
64. Kim JK, Kolodziejczyk AA, Ilicic T, Teichmann SA, and Marioni JC (2015). Characterizing noise structure in single-cell RNA-seq distinguishes genuine from technical stochastic allelic expression. Nat Commun 6, 8687. 10.1038/ncomms9687. [PubMed: 26489834]
65. Brennan MD, Cheong R, and Levchenko A (2012). How Information Theory Handles Cell Signaling and Uncertainty. Science 338, 334–335. 10.1126/science.1227946. [PubMed: 23087235]
66. Jetka T, Nienałtowski K, Filippi S, Stumpf MPH, and Komorowski M (2018). An information-theoretic framework for deciphering pleiotropic and noisy biochemical signaling. Nature Communications 9, 4591. 10.1038/s41467-018-07085-1.
67. Jetka T, Nienałtowski K, Winarski T, Błoński S, and Komorowski M (2019). Information-theoretic analysis of multivariate single-cell signaling responses. PLoS Comput Biol 15, e1007132. 10.1371/journal.pcbi.1007132. [PubMed: 31299056]

68. Komorowski M, and Tawfik DS (2019). The Limited Information Capacity of Cross-Reactive Sensors Drives the Evolutionary Expansion of Signaling. Cell Systems 8, 76–85.e6. 10.1016/j.cels.2018.12.006. [PubMed: 30660612]
69. Tang Y, Adelaja A, Ye FX-F, Deeds E, Wollman R, and Hoffmann A (2021). Quantifying information accumulation encoded in the dynamics of biochemical signaling. Nature Communications 12, 1272. 10.1038/s41467-021-21562-0.
70. Uda S, Saito TH, Kudo T, Kokaji T, Tsuchiya T, Kubota H, Komori Y, Ozaki Y, and Kuroda S (2013). Robustness and compensation of information transmission of signaling pathways. Science 341, 558–561. 10.1126/science.1234511. [PubMed: 23908238]
71. Caldwell AB, Cheng Z, Vargas JD, Birnbaum HA, and Hoffmann A (2014). Network dynamics determine the autocrine and paracrine signaling functions of TNF. Genes Dev. 28, 2120–2133. 10.1101/gad.244749.114. [PubMed: 25274725]
72. Tkačik G, and Walczak AM (2011). Information transmission in genetic regulatory networks: a review. J. Phys.: Condens. Matter 23, 153102. 10.1088/0953-8984/23/15/153102. [PubMed: 21460423]
73. Tkačik G, Callan CG, and Bialek W (2008). Information capacity of genetic regulatory elements. Phys. Rev. E 78, 011910. 10.1103/PhysRevE.78.011910.
74. Maity A, and Wollman R (2020). Information transmission from NFkB signaling dynamics to gene expression. PLOS Computational Biology 16, e1008011. 10.1371/journal.pcbi.1008011. [PubMed: 32797040]
75. Mukund A, and Bintu L (2022). Temporal signaling, population control, and information processing through chromatin-mediated gene regulation. Journal of Theoretical Biology 535, 110977. 10.1016/j.jtbi.2021.110977. [PubMed: 34919934]
76. Rieckh G, and Tkačik G (2014). Noise and Information Transmission in Promoters with Multiple Internal States. Biophysical Journal 106, 1194–1204. 10.1016/j.bpj.2014.01.014. [PubMed: 24606943]
77. Bintu L, Yong J, Antebi YE, McCue K, Kazuki Y, Uno N, Oshimura M, and Elowitz MB (2016). Dynamics of epigenetic regulation at the single-cell level. Science 351, 720–724. 10.1126/science.aab2956. [PubMed: 26912859]
78. Lavin Y, Winter D, Blecher-Gonen R, David E, Keren-Shaul H, Merad M, Jung S, and Amit I (2014). Tissue-Resident Macrophage Enhancer Landscapes Are Shaped by the Local Microenvironment. Cell 159, 1312–1326. 10.1016/j.cell.2014.11.018. [PubMed: 25480296]
79. Davies AE, Pargett M, Siebert S, Gillies TE, Choi Y, Tobin SJ, Ram AR, Murthy V, Juliano C, Quon G, et al. (2020). Systems-Level Properties of EGFR-RAS-ERK Signaling Amplify Local Signals to Generate Dynamic Gene Expression Heterogeneity. cels 11, 161–175.e5. 10.1016/j.cels.2020.07.004.
80. Faure AJ, Schmiedel JM, and Lehner B (2017). Systematic Analysis of the Determinants of Gene Expression Noise in Embryonic Stem Cells. Cell Systems 5, 471–484.e4. 10.1016/j.cels.2017.10.003. [PubMed: 29102610]
81. Topolewski P, Zakrzewska KE, Walczak J, Nienałtowski K, Müller-Newen G, Singh A, and Komorowski M (2022). Phenotypic variability, not noise, accounts for most of the cell-to-cell heterogeneity in IFN-γ and oncostatin M signaling responses. Sci Signal 15, eabd9303. 10.1126/scisignal.abd9303. [PubMed: 35167339]
82. Brown CR, and Boeger H (2014). Nucleosomal promoter variation generates gene expression noise. Proc Natl Acad Sci U S A 111, 17893–17898. 10.1073/pnas.1417527111. [PubMed: 25468975]
83. Brown CR, Mao C, Falkovskaia E, Jurica MS, and Boeger H (2013). Linking Stochastic Fluctuations in Chromatin Structure and Gene Expression. PLOS Biology 11, e1001621. 10.1371/journal.pbio.1001621. [PubMed: 23940458]
84. Elowitz MB, Levine AJ, Siggia ED, and Swain PS (2002). Stochastic Gene Expression in a Single Cell. Science 297, 1183–1186. 10.1126/science.1070919. [PubMed: 12183631]
85. Swain PS, Elowitz MB, and Siggia ED (2002). Intrinsic and extrinsic contributions to stochasticity in gene expression. PNAS 99, 12795–12800. 10.1073/pnas.162041399. [PubMed: 12237400]

86. Okabe Y, and Medzhitov R (2014). Tissue-specific signals control reversible program of localization and functional polarization of macrophages. Cell 157, 832–844. 10.1016/j.cell.2014.04.016. [PubMed: 24792964]

87. van Beek AA, Van den Bossche J, Mastroberardino PG, de Winther MPJ, and Leenen PJM (2019). Metabolic Alterations in Aging Macrophages: Ingredients for Inflammaging? Trends in Immunology 40, 113–127. 10.1016/j.it.2018.12.007. [PubMed: 30626541]

88. Cui C, Driscoll RK, Piao Y, Chia CW, Gorospe M, and Ferrucci L (2019). Skewed macrophage polarization in aging skeletal muscle. Aging Cell 18, e13032. 10.1111/acel.13032. [PubMed: 31478346]

89. Weisberg SP, McCann D, Desai M, Rosenbaum M, Leibel RL, and Ferrante AW (2003). Obesity is associated with macrophage accumulation in adipose tissue. J Clin Invest 112, 1796–1808. 10.1172/JCI19246. [PubMed: 14679176]

90. Galli SJ, Borregaard N, and Wynn TA (2011). Phenotypic and functional plasticity of cells of innate immunity: macrophages, mast cells and neutrophils. Nat Immunol 12, 1035–1044. 10.1038/ni.2109. [PubMed: 22012443]

91. Cassetta L, Fragkogianni S, Sims AH, Swierczak A, Forrester LM, Zhang H, Soong DYH, Cotechini T, Anur P, Lin EY, et al. (2019). Human Tumor-Associated Macrophage and Monocyte Transcriptional Landscapes Reveal Cancer-Specific Reprogramming, Biomarkers, and Therapeutic Targets. Cancer Cell 35, 588–602.e10. 10.1016/j.ccell.2019.02.009. [PubMed: 30930117]

92. Cohen YC, Zada M, Wang S-Y, Bornstein C, David E, Moshe A, Li B, Shlomi-Loubaton S, Gatt ME, Gur C, et al. (2021). Identification of resistance pathways and therapeutic targets in relapsed multiple myeloma patients through single-cell sequencing. Nature Medicine, 1–13. 10.1038/s41591-021-01232-w.

93. Chang Y-L, Rossetti M, Gjertson DW, Rubbi L, Thompson M, Montoya DJ, Morselli M, Ruffin F, Hoffmann A, Pellegrini M, et al. (2021). Human DNA methylation signatures differentiate persistent from resolving MRSA bacteremia. Proc. Natl. Acad. Sci. U.S.A 118, e2000663118. 10.1073/pnas.2000663118. [PubMed: 33649198]

94. Burel JG, Pomaznoy M, Lindestam Arlehamn CS, Weiskopf D, da Silva Antunes R, Jung Y, Babor M, Schulten V, Seumois G, Greenbaum JA, et al. (2019). Circulating T cell-monocyte complexes are markers of immune perturbations. eLife 8, e46045. 10.7554/eLife.46045. [PubMed: 31237234]

95. Gratchev A, Sobenin I, Orekhov A, and Kzhyshkowska J (2012). Monocytes as a diagnostic marker of cardiovascular diseases. Immunobiology 217, 476–482. 10.1016/j.imbio.2012.01.008. [PubMed: 22325375]

96. Kapellos TS, Bonaguro L, Gemünd I, Reusch N, Saglam A, Hinkley ER, and Schultze JL (2019). Human Monocyte Subsets and Phenotypes in Major Chronic Inflammatory Diseases. Frontiers in Immunology 10.

97. Mathai SK, Gulati M, Peng X, Russell TR, Shaw AC, Rubinowitz AN, Murray LA, Siner JM, Antin-Ozerkis DE, Montgomery RR, et al. (2010). Circulating monocytes from systemic sclerosis patients with interstitial lung disease show an enhanced profibrotic phenotype. Lab Invest 90, 812–823. 10.1038/labinvest.2010.73. [PubMed: 20404807]

98. Patel VK, Williams H, Li SCH, Fletcher JP, and Medbury HJ (2017). Monocyte inflammatory profile is specific for individuals and associated with altered blood lipid levels. Atherosclerosis 263, 15–23. 10.1016/j.atherosclerosis.2017.05.026. [PubMed: 28570862]

99. Brodin P (2021). Immune determinants of COVID-19 disease presentation and severity. Nature Medicine 27, 28–33. 10.1038/s41591-020-01202-8.

100. Brodin P (2022). SARS-CoV-2 infections in children: understanding diverse outcomes. Immunity 0. 10.1016/j.immuni.2022.01.014.

101. Laing AG, Lorenc A, I. del Molino del Barrio, Das A, Fish M, Monin L, Muñoz-Ruiz M, McKenzie DR, Hayday TS, Francos-Quijorna I, et al. (2020). A dynamic COVID-19 immune signature includes associations with poor prognosis. Nature Medicine, 1–13. 10.1038/s41591-020-1038-6.

102. Liu C, Martins AJ, Lau WW, Rachmaninoff N, Chen J, Imberti L, Mostaghimi D, Fink DL, Burbelo PD, Dobbs K, et al. (2021). Time-resolved systems immunology reveals a late juncture

linked to fatal COVID-19. Cell 184, 1836–1857.e22. 10.1016/j.cell.2021.02.018. [PubMed: 33713619]

103. Scully EP, Haverfield J, Ursin RL, Tannenbaum C, and Klein SL (2020). Considering how biological sex impacts immune responses and COVID-19 outcomes. Nature Reviews Immunology 20, 442–447. 10.1038/s41577-020-0348-8.
104. Carvalho K, Rebboah E, Jansen C, Williams K, Dowey A, McGill C, and Mortazavi A (2021). Uncovering the Gene Regulatory Networks Underlying Macrophage Polarization Through Comparative Analysis of Bulk and Single-Cell Data. bioRxiv, 2021.01.20.427499. 10.1101/2021.01.20.427499.
105. Albert-Vega C, Tawfik DM, Trouillet-Assant S, Vachot L, Mallet F, and Textoris J (2018). Immune Functional Assays, From Custom to Standardized Tests for Precision Medicine. Frontiers in Immunology 9.
106. Boomer JS, To K, Chang KC, Takasu O, Osborne DF, Walton AH, Bricker TL, Jarman SD, Kreisel D, Krupnick AS, et al. (2011). Immunosuppression in patients who die of sepsis and multiple organ failure. JAMA 306, 2594–2605. 10.1001/jama.2011.1829. [PubMed: 22187279]
107. Morris AC, Brittan M, Wilkinson TS, McAuley DF, Antonelli J, McCulloch C, Barr LC, McDonald NA, Dhaliwal K, Jones RO, et al. (2011). C5a-mediated neutrophil dysfunction is RhoA-dependent and predicts infection in critically ill patients. Blood 117, 5178–5188. 10.1182/blood-2010-08-304667. [PubMed: 21292772]
108. Urrutia A, Duffy D, Rouilly V, Posseme C, Djebali R, Illanes G, Libri V, Albaud B, Gentien D, Piasecka B, et al. (2016). Standardized Whole-Blood Transcriptional Profiling Enables the Deconvolution of Complex Induced Immune Responses. Cell Rep 16, 2777–2791. 10.1016/j.celrep.2016.08.011. [PubMed: 27568558]
109. Kuhn M (2008). Building Predictive Models in R Using the caret Package. Journal of Statistical Software 28, 1–26. 10.18637/jss.v028.i05. [PubMed: 27774042]
110. Stuart T, Butler A, Hoffman P, Hafemeister C, Papalexi E, Mauck WM, Hao Y, Stoeckius M, Smibert P, and Satija R (2019). Comprehensive Integration of Single-Cell Data. Cell 177, 1888–1902.e21. 10.1016/j.cell.2019.05.031. [PubMed: 31178118]
111. Robinson MD, McCarthy DJ, and Smyth GK (2010). edgeR: a Bioconductor package for differential expression analysis of digital gene expression data. Bioinformatics 26, 139–140. 10.1093/bioinformatics/btp616. [PubMed: 19910308]
112. Heinz S, Benner C, Spann N, Bertolino E, Lin YC, Laslo P, Cheng JX, Murre C, Singh H, and Glass CK (2010). Simple Combinations of Lineage-Determining Transcription Factors Prime cis-Regulatory Elements Required for Macrophage and B Cell Identities. Molecular Cell 38, 576–589. 10.1016/j.molcel.2010.05.004. [PubMed: 20513432]
113. Li J, Bien J, and Wells MT (2018). rTensor: An R Package for Multidimensional Array (Tensor) Unfolding, Multiplication, and Decomposition. Journal of Statistical Software 87, 1–31. 10.18637/jss.v087.i10.
114. Yu G, Wang L-G, Han Y, and He Q-Y (2012). clusterProfiler: an R Package for Comparing Biological Themes Among Gene Clusters. OMICS: A Journal of Integrative Biology 16, 284–287. 10.1089/omi.2011.0118. [PubMed: 22455463]
115. Lin L, Song M, Jiang Y, Zhao X, Wang H, and Zhang L (2020). Normalizing single-cell RNA sequencing data with internal spike-in-like genes. NAR Genomics and Bioinformatics 2. 10.1093/nargab/lqaa059.
116. Tucker LR (1966). Some mathematical notes on three-mode factor analysis. Psychometrika 31, 279–311. 10.1007/BF02289464. [PubMed: 5221127]
117. Wang N, Lefaudeux D, Mazumder A, Li JJ, and Hoffmann A (2021). Identifying the combinatorial control of signal-dependent transcription factors. PLOS Computational Biology 17, e1009095. 10.1371/journal.pcbi.1009095. [PubMed: 34166361]

**Highlights:**

- Macrophages mount pathogen/stimulus-specific responses, but how specific are they?
- An experimental and computational workflow to quantify Response Specificity
- Response Specificity is distinctively altered by microenvironmental cytokines
- The R-S-Index quantifies macrophage functional states in old and obese mice

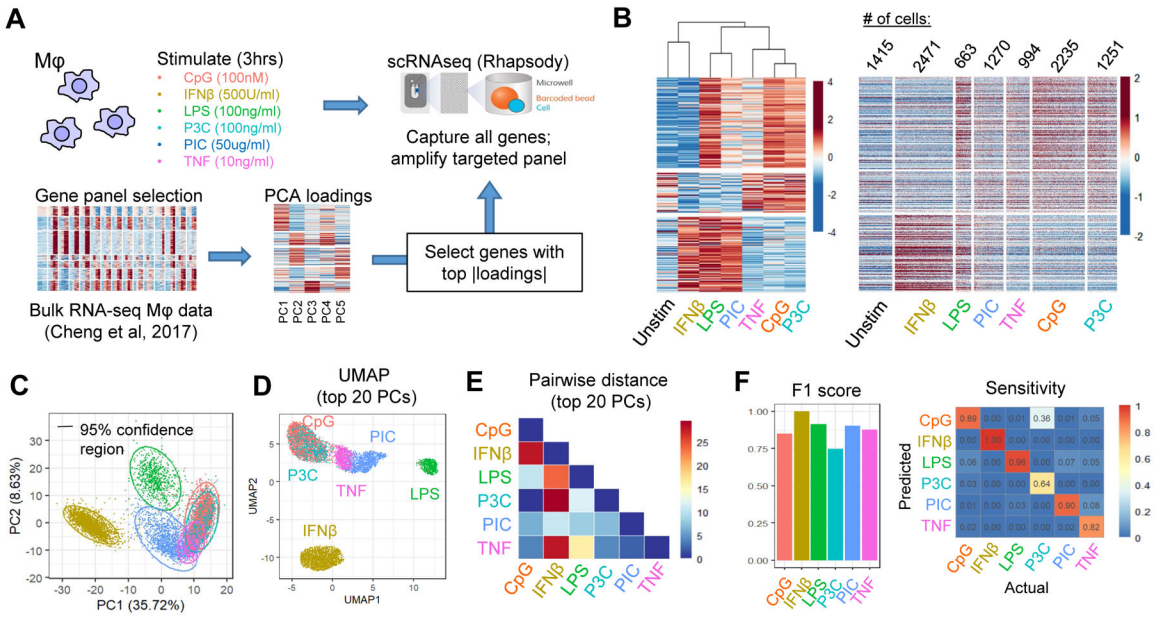


**Figure 1. Macrophages produce highly specific gene expression responses to diverse immune stimuli.**

A. A cost-effective experimental workflow using targeted single-cell RNA-sequencing profiles immune response gene expression at single cell resolution. Bottom left: Heatmap of all genes induced with log2(FC)>2 in any stimulus from bulk RNAseq data (Cheng et al, 2017). Bottom middle: PCA loadings from bulk RNAseq data. Bottom right: Panel genes were selected by scoring each gene based on the summed strength of the loadings from the top 20 PCs. Top right: All genes are captured, and selected genes are amplified via a targeted primer panel.

B. Comparison of bulk RNAseq data and single cell data shows concordance of gene expression clusters, and also reveals single cell heterogeneity. Color bars represent z-scores.

C. PCA on macrophages stimulated for 3 hours indicates there may be a high degree of stimulus-specificity despite single cell heterogeneity, but TNF, P3C and CpG appear overlapping on the first two components. Ellipses represent 95% confidence intervals based on multivariate t-distribution. Colors are the same as in Figure 1A.

D. UMAP of stimulated macrophages using the top 20 PCA components clarifies that TNF can be separated, but P3C and CpG response distributions remain overlapping.

E. Calculation of the Bhattacharya distance between pairs of response distributions confirms the similarity of CpG and P3C distributions. IFNβ is the most distinct from all other stimuli, but with a response-distribution space closest to that of PIC. Bhattacharya distances were calculated on the top 20 principal components.

F. A random forest classifier confirms high identifiability of each stimulus condition, with only the bacterial ligands P3C and CpG being confused with each other. Classifier was trained on 70% of all single cell data (2 replicate experiments from M0 naïve macrophage populations) and tested on the remaining 30% of held-out data. Color bar represents sensitivity.

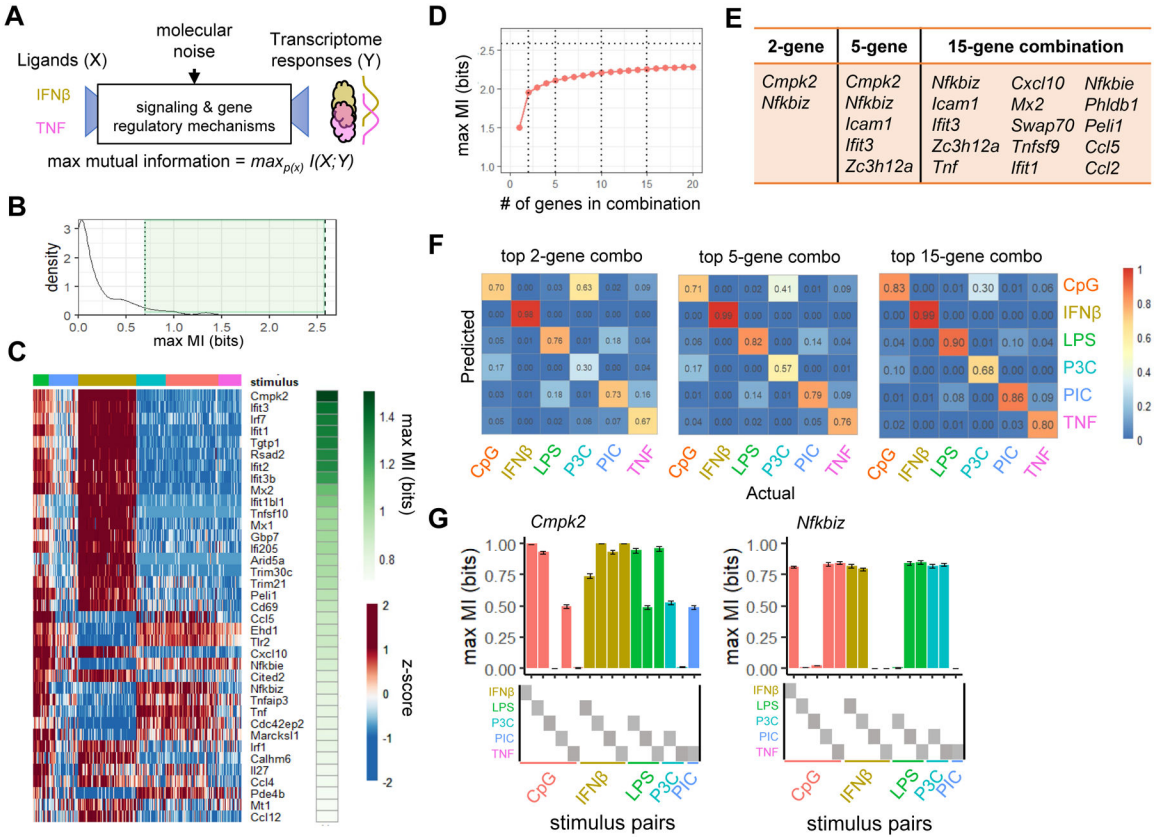


**Figure 2. Despite high stimulus-specificity of gene expression programs, individual genes are capable of distinguishing only a subset of stimulus pairs.**

A. An information theoretic approach treats single cell signaling and epigenetic mechanisms as a communication channel that passes extracellular information to nuclear target genes.

B. Distribution of max MI values for single genes shows that only a few genes have a max MI above 1 bit, with 1 bit indicating the ability to distinguish two groups. Highlighted in green are high max MI genes shown in the heatmap in Figure 2C.

C. Heatmap of single cell gene expression indicates that low max MI is because most genes have binary expression patterns, on or off, rather than a range of levels that would have been able to distinguish multiple groups of stimuli.

D. Max MI as a function of the indicated number of genes in combination, for the gene combinations providing the highest max MI. Horizontal dotted line indicates theoretical limit for 6 stimuli.

E. Gene names for the combinations that allow for the highest max MI for each given number of genes.

F. Confusion matrices from random forest classifiers for gene combinations indicate that a small number of genes generates fair prediction accuracy, and a classifier trained on 15 genes performs approximately the same as all genes.

G. The genes comprising the top 2-gene combination, *Cmpk2* and *Nfkbiz*, distinguish complementary stimulus-pairs. Error bars represent standard deviations from 10 iterations of 50% bootstrap resampling of the single cell data.

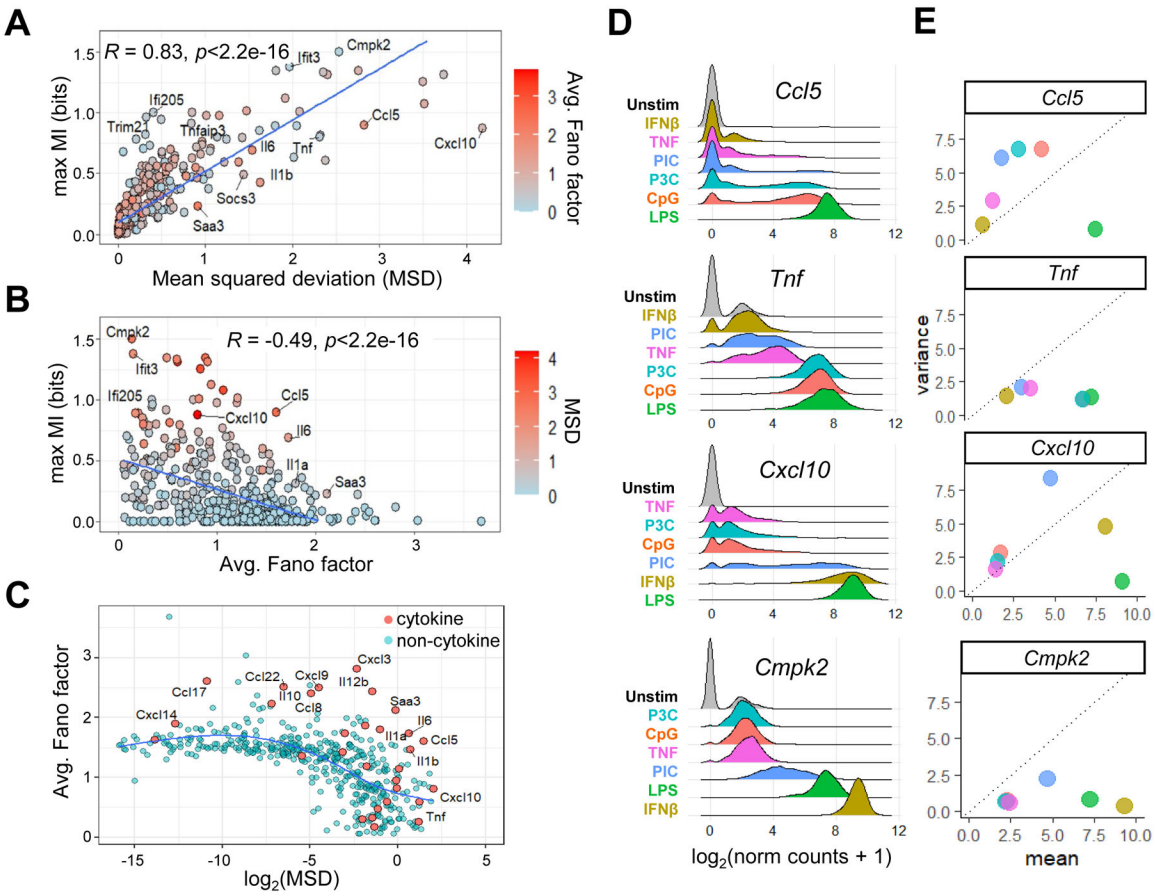


**Figure 3. The Response Specificity of cytokine genes is limited by cell-to-cell heterogeneity, despite having distinct expression means.**

A. Deviation in mean expression among the six stimuli plotted against max MI for each gene. Genes are colored by their average amount of dispersion across the six stimuli (average Fano Factor).

B. Average Fano Factor across the six stimuli plotted against max MI shows genes with high or low dispersion. Genes are colored by deviation in mean expression across stimuli (mean squared deviation).

C. Mean squared deviation vs. average Fano factor over all stimuli, with cytokine genes highlighted.

D. Expression distributions of cytokine (*Ccl5*, *Tnf*, *Cxcl10*) and non-cytokine (*Cmpk2*) genes, showing distinct variance of responses to each stimulus.

E. Mean expression level vs. expression variance for each stimulus-response distribution. Dotted lines mark where variance equals mean.

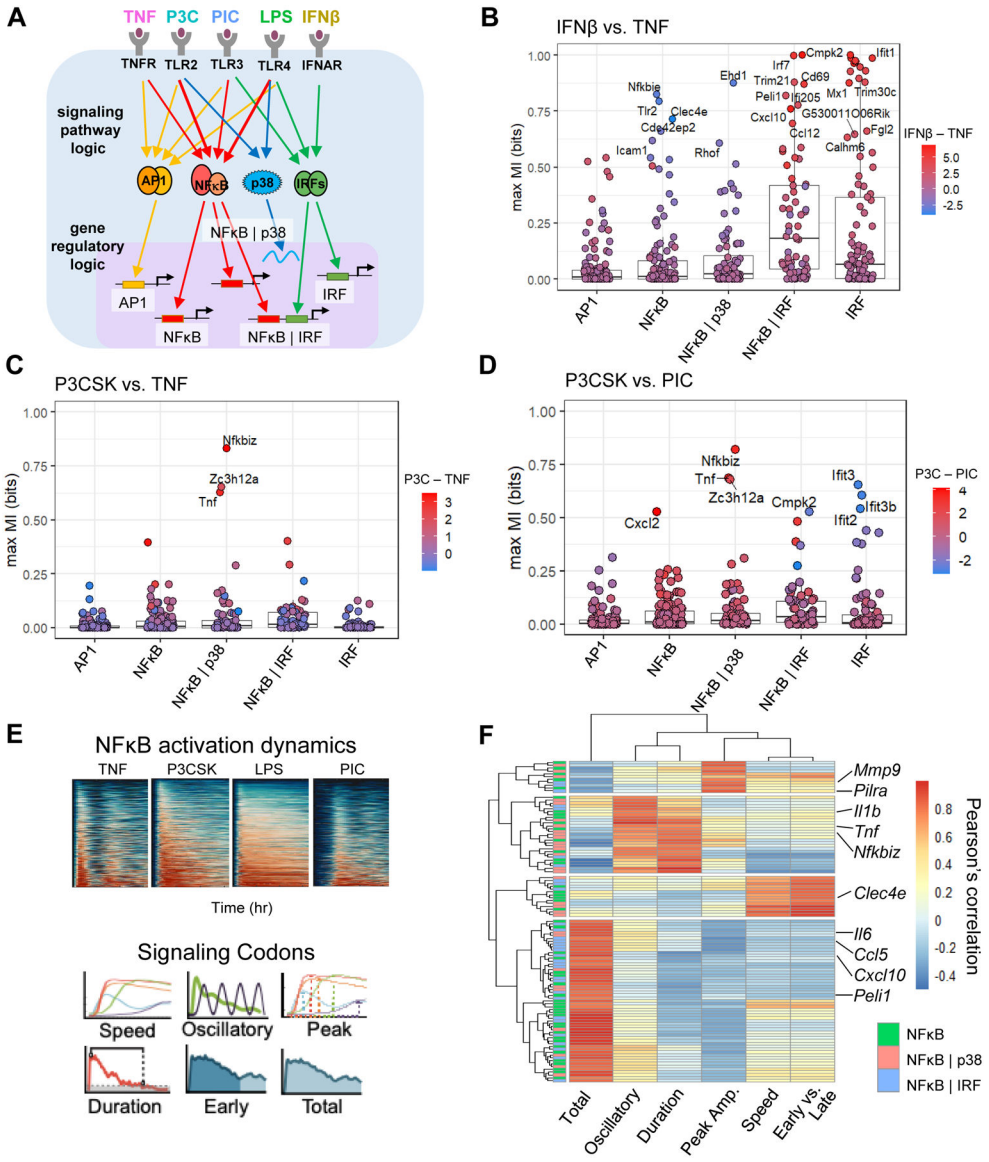


**Figure 4. Stimulus specificity of immune response genes from selective deployment of IRF and p38 pathways, and NFκB dynamical features.**

A. Signaling and gene regulatory mechanisms are responsible for generating Response Specificity. MAPKp38, IRF3, AP1, and NFκB signaling profiles are activated in response to inflammatory stimuli and act in combination to regulate gene expression, using five identified regulatory logics (Cheng et al., 2017).

B. Distribution of max MI values for genes of the five regulatory logics for IFNβ vs. TNF.

C. Distribution of max MI values for genes of the five regulatory logics for P3CSK vs. TNF.

D. Distribution of max MI values for genes of the five regulatory logics for P3CSK vs. PIC.

E. Single-cell NFκB signaling dynamics in response to TNF, P3CSK, LPS, or PIC. Heatmap represents nuclear NFκB concentration. Information conveyed by NFκB dynamical activity is transmitted through six NFκB signaling codons (Adelaja et al., 2021).

F. Response Specificity of NFκB target genes across all pairs of stimuli vs. stimulus-specificity in NFκB signaling codons. Color represents correlation strength between pairwise gene expression and pairwise signaling codon Response Specificity.

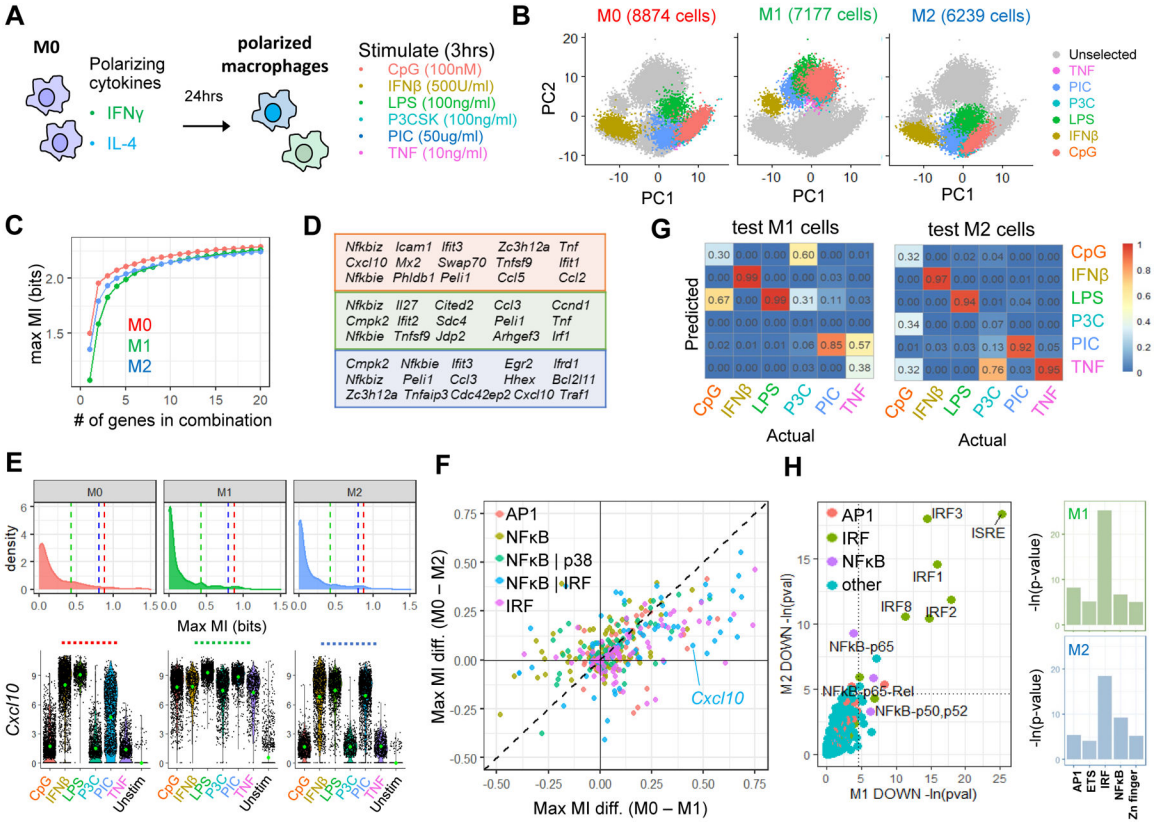


**Figure 5. Cytokine polarization causes complex modulation of the Response Specificity of specific genes to specific stimuli**

A. The Response Specificity experimental assay captures response distributions to six stimuli in M1(IFNγ) and M2(IL4) polarized macrophages.

B. PCA on all M0, M1(IFNγ), and M2(IL4) macrophage responses to the six stimuli. Variance explained by PC1 (19.9%), by PC2 (15.7%). Polarized macrophages produce response distributions distinct from those of M0 macrophages.

C. Response Specificity as calculated by max MI is slightly reduced in both M1(IFNγ) and M2(IL4) polarization states, for every dimension of best possible gene combinations.

D. Genes within the best 15-gene combination for M0, M1(IFNγ), and M2(IL4) macrophages are distinct.

E. Top: Distribution of max MI values of individual genes for M0, M1(IFNγ), and M2(IL4) macrophage responses. Dotted lines mark the max MI of *Cxcl10* for each macrophage state: red (M0), green (M1), blue (M2). Bottom: *Cxcl10* stimulus-response distributions for M0 (left), M1 (center) and M2 (right) macrophage states are shown.

F. Scatterplot of differences in max MI values between M0 vs. M1(IFNγ) or M2(IL4) macrophage responses. Genes are colored by assigned gene regulatory logic.

G. Confusion matrices representing the accuracy of stimulus prediction, given single cell gene expression profiles for M1 and M2 macrophages, using the random forest model trained on naïve M0 macrophages. Color bar represents sensitivity.

H. Motifs that lose specificity in M1 or M2 macrophages compared to M0 naïve macrophages. Left: Enrichments of all potential motifs. Right: Barplot of most significant enrichment for each motif category.

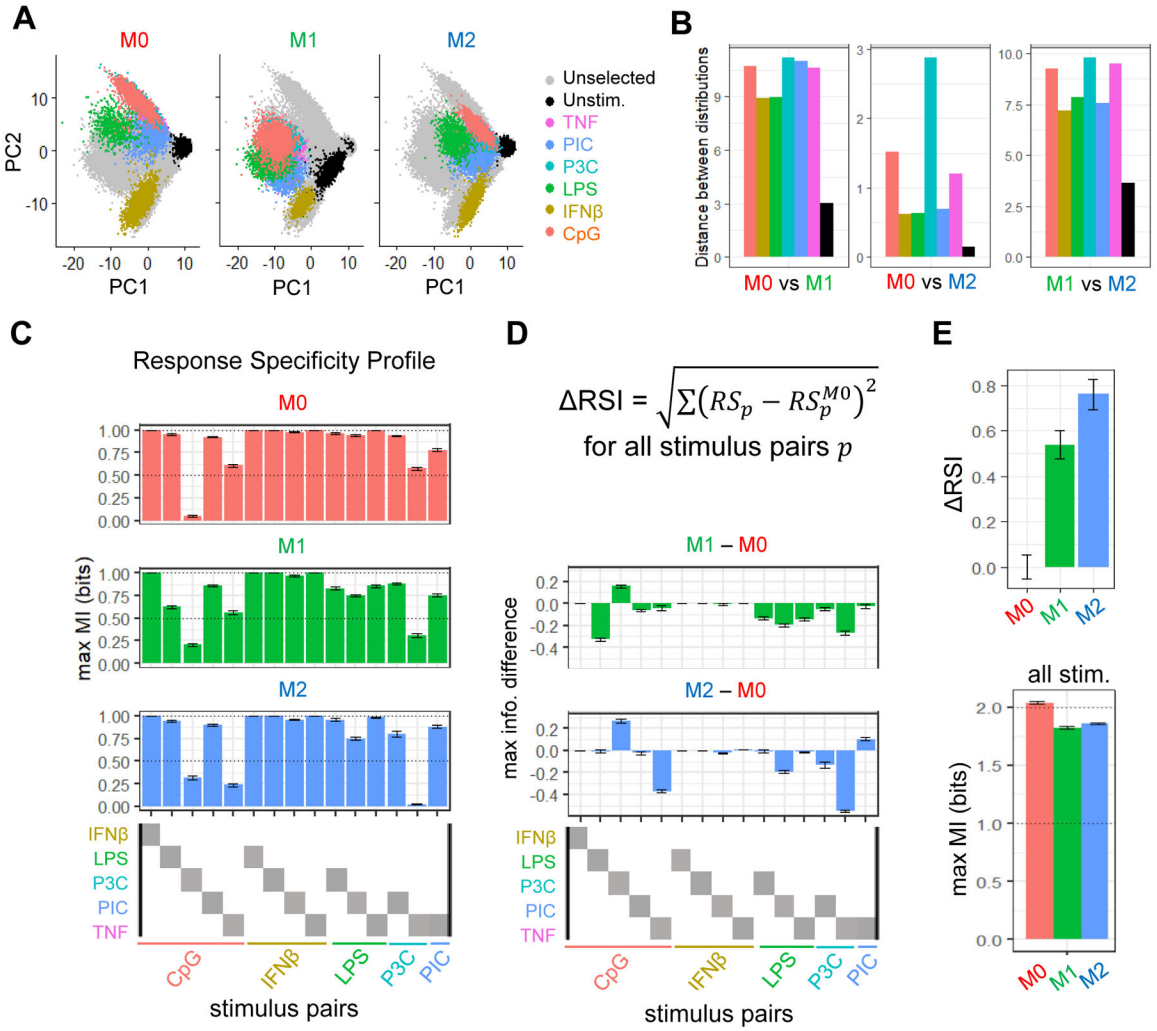


**Figure 6. The Response Specificity Profile of stimulus pairs assesses the functional state of macrophages, and readily distinguishes M0 vs. M1 vs. M2.**

A. PCA of stimulus responses vs. resting state expression profiles of M0 vs. M1 vs. M2 macrophages.

B. Quantification of differences in response distributions vs. resting state distributions among the three macrophage states using Bhattacharyya distance on the first three components. Colors are the same as in Figure 6A.

C. Response Specificity Profiles measured by max mutual information of all 15 stimulus pairs, as defined by response distributions to 6 stimuli. M0, M1, and M2 macrophage responses each show specific differences in select pairs. Error bars represent standard deviations from 50 iterations of 50% bootstrap resampling.

D. Across all pairs, the difference in max MI from M0 responses is calculated to derive delta Response Specificity Index, a characteristic signature of the functional state of the macrophage.

E. Top: A summary of the pair-wise profile into a single number, the delta Response Specificity Index. Bottom: ΔRSI provides a clearer indication of differences than calculating

the mutual information on all stimulus-response datasets together. Error bars for ΔRSI represent propagation of the original standard deviations in max MI calculations.

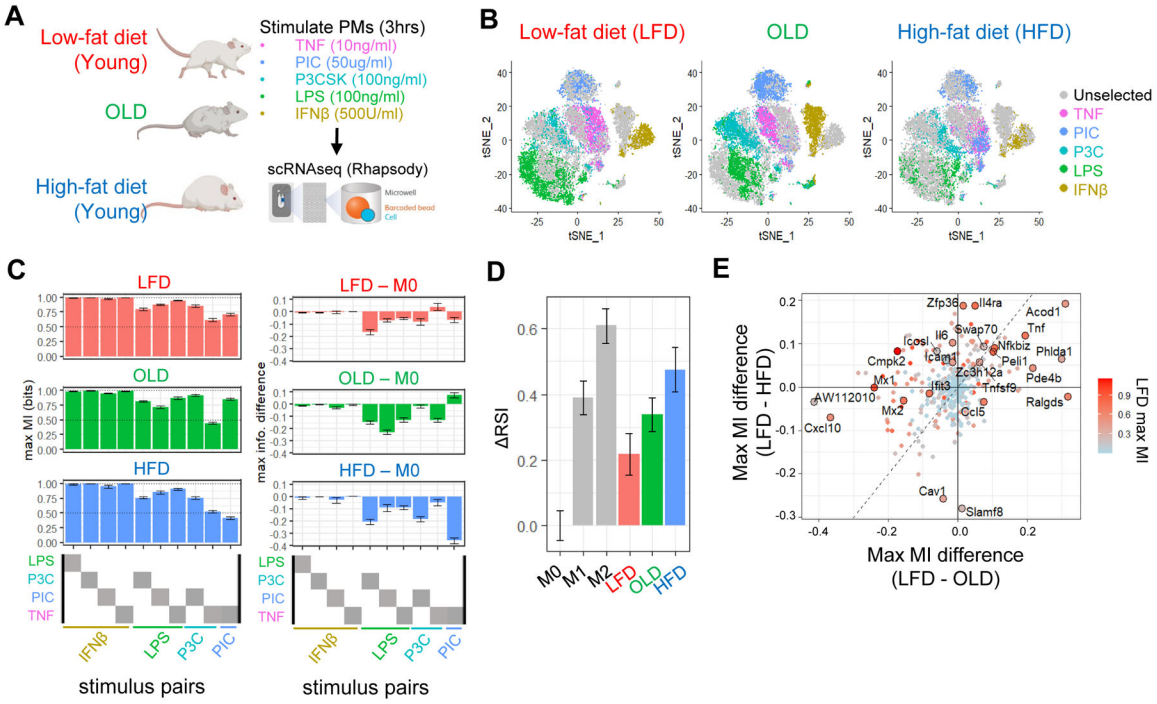


**Figure 7. Old and obese mouse peritoneal macrophages show distinctive alterations in their Response Specificity Profile.**

A. Measuring Response Specificity for three mouse models using peritoneal macrophages: Healthy low-fat diet mice (16wks), old mice (>90wks), and high-fat diet mice (16wks). Cells from two mice were aggregated for each condition.

B. tSNE visualization of peritoneal macrophage responses to stimuli for each of the mouse models, healthy (LFD), OLD, and high-fat diet (HFD), using the top 20 principal components.

C. Left: Macrophage responses from healthy and disease mouse models are scored by the Response Specificity Profile. Error bars represent standard deviations from 50 iterations of 50% bootstrap resampling. Right: Subtracting each profile from the Response Specificity Profile of M0 macrophages highlights pair-wise differences in max MI values.

D. Square root of the sum of the squared deviation from M0 across all stimulus-pairs was calculated to obtain the single-value ΔRSI (Fig. 6B). For both polarized macrophages and peritoneal macrophages, stimulus-pairs that included CpG were not included due to CpG not being used in the Response Specificity assay on peritoneal macrophages. Higher numbers for ΔRSI indicate a larger deviation in Response Specificity Index from M0. Error bars represent propagation of the original standard deviations in max MI calculations.

E. Scatterplot of differences in max MI values between LFD vs. OLD or HFD macrophage responses. Genes are colored by the absolute max MI quantity for each gene in the LFD mouse model.

## KEY RESOURCES TABLE

| REAGENT or RESOURCE | SOURCE | IDENTIFIER |
|---|---|---|
| Antibodies | | |
| Anti-mouse CD45-hashtag antibodies | BD Rhapsody | 633793 |
| | | |
| | | |
| Chemicals, peptides, and recombinant proteins | | |
| LPS | Sigma, B5:055 | L2880 |
| murine TNF | Roche | 11271156001 |
| Pam3CSK4 | Invivogen | tlrl-pms |
| low MW polyinosine-polycytidylic acid (Poly(I:C)) | Invivogen | tlrl-picw |
| synthetic CpG ODN 1668 | Invivogen | tlrl-1668 |
| murine IFNβ | R&D | 12401–1 |
| murine IFNγ | R&D | 485-MI |
| murine IL-4 | R&D | 404-ML |
| | | |
| | | |
| Critical commercial assays | | |
| BD Rhapsody Express Single-Cell Analysis system | BD | 633702 |
| Targeted mRNA and AbSeq Reagent Kit 4 Pack | BD | 633771 |
| BD Rhapsody Cartridge Reagent Kit | BD | 633731 |
| BD Rhapsody Cartridge Kit | BD | 633733 |
| BD Rhapsody cDNA Kit | BD | 633773 |
| BD Rhapsody P5000M pipette | BD | 633705 |
| BD™ Stain Buffer (FBS) | BD Pharmigen | 554656 |
| | | |
| | | |
| Deposited data | | |
| BD Rhapsody scRNAseq processed data | This paper | DOI: 10.5281/zenodo.7296165 https://github.com/signalingsystemslab/ResponseSpecificity |
| BD Rhapsody scRNAseq fastqs | This paper | GSE220970 |
| BMDM bulk RNAseq data | [8] | GSE68318 |
| Single cell NFκB signaling dynamics | [41] | https://doi.org/10.17632/6wksmvh5p4.1 |
| 10× scRNAseq of macrophages | [41] | GSE162992 |
| 10× scRNAseq of peritoneal macrophages | [55] | GSE145562 |
| | | |
| Experimental models: Cell lines | | |
| Immortalized Myeloid Progenitor-derived macrophages | [25] | N/A |
| | | |
| Experimental models: Organisms/strains | | |
| C57BL/6J 90wks old | Jackson Labs | 000664 |
| C57BL/6J/DIO high fat diet (60% fat diet) | Jackson Labs | 380050 |
| C57BL/6J/DIO controls (10% fat diet) | Jackson Labs | 380056 |
| | | |

| REAGENT or RESOURCE | SOURCE | IDENTIFIER |
|---|---|---|
| Oligonucleotides | | |
| Rhapsody Custom Panel: ID 1330 | BD | 633743 |
| Rhapsody Custom Panel: ID 1331 | BD | 633743 |
| Rhapsody Custom Panel: ID 1332 | BD | 633743 |
| Rhapsody Custom Panel: ID 1334 | BD | 633743 |
| Rhapsody Custom Panel: ID 1341 | BD | 633743 |
| | | |
| | | |
| Software and algorithms | | |
| CARET | [109] | http://caret.r-forge.r-project.org/ |
| Seurat | [110] | https://www.rdocumentation.org/packages/Seurat/versions/3.1.4 |
| BD Rhapsody Targeted Analysis Pipeline (version v1.0) | [23] | https://www.sevenbridges.com/ |
| *edgeR* | [111] | https://bioconductor.org/packages/release/bioc/html/edgeR.html |
| HOMER | [112] | http://homer.ucsd.edu/homer/ |
| SLEMI | [67] | https://cran.r-project.org/web/packages/SLEMI/index.html |
| rtensor | [113] | https://cran.r-project.org/web/packages/rTensor/index.html |
| clusterProfiler | [114] | https://bioconductor.org/packages/release/bioc/html/clusterProfiler.html |
| ISnorm | [115] | PMID 33575610, PMC7671304 |
| Code for machine learning and Response Specificity Profile | This paper | DOI: 10.5281/zenodo.7296165 https://github.com/signalingsystemslab/ResponseSpecificity |